This article has been accepted for publication in a future issue of this journal, but has not been fully edited. Content may change prior to final publication. Citation information: DOI 10.1109/TSG.2019.2920362, IEEE Transactions on Smart Grid

Chance-Constrained Frequency Regulation with Energy Storage Systems in Distribution Networks

Yanan Sun, *Student Member, IEEE*, Shahab Bahrami, *Member, IEEE*,
Vincent W.S. Wong, *Fellow, IEEE*, and Lutz Lampe, *Senior Member, IEEE*

***Abstract*—One of the applications of energy storage systems (ESSs) is to support frequency regulation in power systems. In this paper, we consider such an application and address the challenges of uncertain frequency changes, limited energy storage, as well as distribution network constraints. We formulate a bi-level optimization problem that includes the operation objectives of the system operator and the ESSs, using chance constraints to account for uncertain frequency changes. The frequency regulation decision of the system operator depends on the ESSs decision to participate in the regulation service as well as the distribution network constraints. Due to the interdependencies between the ESSs demand fluctuations and the distribution network power flow changes, the system operator requires the ESSs' operation information for frequency regulation decisions, which may not be available from the ESSs. Therefore, we propose a decentralized algorithm such that the system operator and the ESSs can pursue their own operation objectives, while ensuring the distribution network constraints are satisfied. We evaluate the performance of our method on IEEE 37-bus and 123-bus test feeders by considering combinations of ESSs with different sizes. Simulation results demonstrate that our approach can successfully coordinate the ESSs to regulate the frequency deviations.**

***Index Terms*—Frequency regulation, energy storage systems, distribution network, chance constraint, bi-level optimization.**

I. Introduction

The fast proliferation of the intermittent renewable generation increases the amount of disturbances in power systems that affect the system frequency. Frequency regulation maintains the power system frequency around the nominal value by compensating generation-load mismatch [1]. Traditionally, regulation capacity has been largely provided by conventional generators. However, the ramping capabilities of conventional generators limit their participation in frequency regulation. The recent advancement of new technologies such as energy storage systems (ESSs) presents new opportunities for frequency regulation service [2], [3]. The wide range of battery power rating and response speed makes ESSs an attractive alternative to provide regulation service [4]. The United States (U.S.) Federal Energy Regulatory Commission (FERC) recently issued Order 841 to remove barriers for the ESSs to participate in the ancillary services market [5]. With the steep decline in the cost of ESSs, the FERC Order 841 will foster the adoption and deployment of ESSs to provide frequency regulation service [5].

There has been a rich body of literature on exploiting the ESSs for frequency regulation service. These works address various issues on the market economics, system integration, as well as the technical and operational challenge of using the ESSs in standard practice. The regulatory policy changes to facilitate the ESSs participation in the marketplace have been discussed in [6], [7]. Different market schemes for the ESSs to participate in frequency regulation have been studied in [8]. The control and coordination schemes of the ESSs with other resources (e.g., conventional generators, wind turbines) for regulation service at the grid-level have been investigated in [9]–[15]. Various battery technologies and control strategies for efficient ESSs operation to provide frequency regulation have been proposed in [16]–[20]. The aforementioned works focus on the ESSs' decision to maximize their participation in regulation service by leveraging the market structure and tackling the operation challenges to provide frequency regulation.

In this paper, we focus on the system operator's decision-making when using the ESSs for frequency regulation, which takes into account the ESSs' operation economics. We adopt a hierarchical decision-making structure based on bi-level optimization, such that the system operator and the ESSs can pursue their own objective, subject to the operation constraints. Bi-level programming has been applied in decision-making when using the ESSs for various aspects in power systems planning and operation [21]–[24]. The ESS investment decisions under different market operation scenarios are studied in [21]. The bidding strategy of an electric vehicle (EV) aggregator to participate in the day-ahead market is proposed in [22]. The strategic behavior of a player with ESSs in the wholesale electricity market is investigated in [23]. A market-based approach to minimize the cost of distribution system operation that accommodates customers' reliability preference is proposed in [24]. Our paper is different from [21]–[24] as we address the specific technical challenge for the application of ESSs for frequency regulation.

A major challenge for the system operator to use ESSs for frequency regulation arises from the uncertain frequency changes and the limited storage capacity. The ESSs' regulation performance can be largely affected by their physical operation constraints and the uncertain frequency changes in the power systems, e.g., the future participation of the ESSs in the regulation service when needed will be limited if their capacity is saturated. One common approach to mitigate the aforementioned issues is using chance constraints to handle

Y. Sun, S Bahrami, V.W.S Wong, and L. Lampe are with the Department of Electrical and Computer Engineering, The University of British Columbia, Vancouver, Canada, email:{ynsun, bahramis, vincentw, lampe}@ece.ubc.ca.
This work was supported by the Natural Sciences and Engineering Research Council of Canada (NSERC).

This article has been accepted for publication in a future issue of this journal, but has not been fully edited. Content may change prior to final publication. Citation information: DOI 10.1109/TSG.2019.2920362, IEEE Transactions on Smart Grid

the uncertainties. Chance-constrained optimization has been applied to design risk-averse strategy for the ESSs in various contexts [25]–[29]. A chance-constrained optimal power flow model is proposed in [25] to minimize the cost for the system operator's redispacth to correct energy imbalance. A risk-averse capacity offering strategy for an aggregator that operates distributed energy resources (DERs) is proposed in [26] based on chance-constrained programming. An optimal bidding strategy for an EV aggregator to participate in the day-ahead market is proposed in [27], which incorporates a chance constraint to capture the EV uncertainty. An online optimal controller for microgrids is designed in [28] based on stochastic chance-constrained optimization. A chance-constrained co-optimization framework that takes into account the ESSs' recharging strategy for primary frequency control service is presented in [29]. Following similar approach, we alleviate the challenge associated with limited ESSs storage for frequency regulation by introducing a chance constraint to address the uncertain frequency changes.

Besides addressing the operation economics and technical challenges for the system operator to use the ESSs for frequency regulation, another major focus in this paper is on the prospect of leveraging the ESSs in the distribution network to participate in and contribute to regulation service. With the increased penetration of DERs and behind-of-the-meter ESSs installed by industrial customers, the system operator can benefit from exploiting these ESSs in the distribution network [30]. New opportunity opens up for the system operator to perform frequency regulation by using the services provided from the distribution network. Therefore, we aim to advance the research efforts by addressing the operation constraints in the distribution network when using the ESSs for the regulation service, as the distribution line limits may affect the ESSs' participation to regulate the system frequency deviations. This differentiates our work from the aforementioned works [10]–[29], as prior research efforts of using the ESSs to provide frequency regulation do not consider the operation constraints imposed by the distribution network.

Incorporating the distribution network constraints when exploiting the ESSs for frequency regulation is nontrivial, mainly due to the interdependencies between the ESSs demand fluctuations and the power flow changes in the distribution network. The ESSs need to adjust their demand to provide regulation service. The change in the ESSs demand will affect the power flow changes in the distribution network. The change in the power flow needs to be feasible, as the power flow limit of the distribution lines cannot be violated when performing frequency regulation. This is further complicated by the interdependencies of the ESS scheduling decisions, i.e., current ESS scheduling decisions affect the availability of stored energy and the participation in the regulation service in the future. Considering the uncertain system frequency changes and the limited energy storage capacity, addressing the distribution network constraints for the ESSs frequency regulation problem becomes very challenging.

In our previous work [31], we have considered the distribution network constraints for the system operator to schedule the ESSs to provide regulation service and proposed a risk-averse solution to minimize the risk of frequency deviation after performing frequency regulation. In this paper, we extend our previous work by considering the operation objective of ESSs for frequency regulation. Our aim is to enlarge the scope of our work given the context that ESSs may be self-interested in providing regulation service, and to render the solution more applicable for the system operator to achieve frequency regulation by exploiting the ESSs in the distribution network. Our main contributions are summarized as follows:

- We propose a bi-level optimization problem for frequency regulation which enables the system operator and the ESSs to pursue their own operation objectives, subject to the operation constraints. In our problem formulation, we incorporate the distribution network constraints to account for their impact on the ESSs' participation in the frequency regulation service.
- We introduce a chance constraint to alleviate the challenge with the ESSs availability for regulation service, considering the uncertain frequency changes. We apply scenario approximation technique to address the nonconvex chance constraint. We derive a tight bound on the number of frequency samples to approximate the chance constraint with a high confidence level.
- We decouple the decision making between the system operator and the ESSs by designing appropriate price signals based on Lagrangian relaxation. We propose a decentralized algorithm based on dual decomposition that can be executed by the ESSs in a distributed and parallel fashion. The proposed algorithm allows the system operator to align with the ESSs on the frequency regulation decisions without knowing the ESSs' operation information, while ensuring the distribution network constraints are satisfied.

We validate our approach by simulations on IEEE 37-bus and 123-bus test feeders using combinations of ESSs with different sizes. Results show that by using our decentralized algorithm, the system operator can successfully regulate the frequency without knowledge about the ESSs' operation information, given the uncertain frequency changes. We demonstrate that the distribution network constraints will affect the flexibility of the ESSs to provide frequency regulation. By using small size ESSs that are scattered in the distribution network, the impact of the power flow constraints on frequency regulation can be reduced.

The rest of the paper is organized as follows. Our system model is introduced in Section II. The bi-level chance-constrained optimization problem and the decentralized algorithm design for the ESSs participation in regulation service are discussed in Section III. Simulation results and performance evaluation of our proposed method are presented in Section IV. Section V concludes the paper.

II. System Model

Consider a distribution network with a set of buses $\mathcal{N}$ and branches $\mathcal{L} \subseteq \mathcal{N} \times \mathcal{N}$. The distribution network consists of some generators, loads, and ESSs. It is connected to the transmission network through a substation bus. The transmission network is modeled by an equivalent virtual generator that

This article has been accepted for publication in a future issue of this journal, but has not been fully edited. Content may change prior to final publication. Citation information: DOI 10.1109/TSG.2019.2920362, IEEE Transactions on Smart Grid

can inject (absorb) active and reactive power into (from) the distribution network. The generator models the power flow between the distribution and transmission networks. A system operator is responsible for monitoring the real-time system operation including frequency changes and power flow. It aims to leverage the ESSs in the distribution network for frequency regulation service if necessary. Let $\mathcal{N}^{\rm s} \subseteq \mathcal{N}$ denote the set of buses with ESSs that participate in regulation service. We divide the operation cycle into a set $\mathcal{T} = \{1, \ldots, T\}$ of T time slots. Each time slot corresponds to a frequency control interval (e.g., 15 minutes). We denote the control interval between two consecutive slots by Δt.

In the following subsections, we discuss how frequency deviation can be regulated by using the ESSs, and present the ESSs and distribution network models.

A. Secondary Frequency Regulation Model

At the beginning of time slot $t \in \mathcal{T}$, if the system encounters a disturbance (e.g., generator failure), the system operator will observe a frequency deviation in the transmission network. Primary frequency control is activated, and the participating generators will respond within few seconds (e.g., 10 seconds) through the governor action [32]. Although the primary frequency control can maintain the frequency within a certain range, it may not be able to restore the system frequency to its nominal value [32]. Let $\Delta\omega(t)$ denote the system frequency deviation from the nominal value after primary frequency control in time slot t. The system operator then leverages the ESSs to perform secondary frequency regulation. Let $\Delta\omega^{\rm reg}(t)$ denote the system frequency change after secondary frequency regulation in time slot t. By coordinating the ESSs' power demand change in each time slot t, the system operator aims to restore the frequency, i.e., $\Delta\omega(t) + \Delta\omega^{\rm reg}(t) = 0$. In practice, however, due to the operation constraints of the ESSs and the distribution network, the system operator allows the regulated frequency at steady state to be within some prescribed limits after performing regulation [33]. Let ϵ denote the maximum acceptable steady state frequency deviation. We have

$$|\Delta\omega(t) + \Delta\omega^{\rm reg}(t)| \le \epsilon, \quad t \in \mathcal{T}, \tag{1}$$

where $|\cdot|$ denotes the absolute value.

a) Regulation Signal Design: To achieve the frequency change $\Delta\omega^{\rm reg}(t)$ in time slot t, the system operator computes the area control error (ACE) signal [34]. The ACE signal determines the amount of active power change for each bus with an ESS. Let $\Delta p_n^{\rm s}(t)$ denote the ACE signal for the ESS at bus $n \in \mathcal{N}^{\rm s}$. The ESS adjusts the power demand $p_n^{\rm s}(t)$ that it can absorb from or inject into the power grid from a scheduled value $\overline{p}_n^{\rm s}(t)$ to provide frequency regulation. We have

$$p_n^{\rm s}(t) = \overline{p}_n^{\rm s}(t) + \Delta p_n^{\rm s}(t). \tag{2}$$

Due to the fluctuations in the ESSs power demand, the power flow in the distribution lines will change. Let $\Delta p_n^{\rm inj}(t)$ denote the change in the injected active power $p_n^{\rm inj}(t)$ at bus n in time slot $t \in \mathcal{T}$ from the scheduled value $\overline{p}_n^{\rm inj}(t)$. That is,

$$p_n^{\rm inj}(t) = \overline{p}_n^{\rm inj}(t) + \Delta p_n^{\rm inj}(t), \quad n \in \mathcal{N}. \tag{3}$$

We have

$$\beta_n \Delta\omega^{\rm reg}(t) = \begin{cases} \Delta p_n^{\rm inj}(t) - \Delta p_n^{\rm s}(t), & \text{if } n \in \mathcal{N}^{\rm s}, \\ \Delta p_n^{\rm inj}(t), & \text{if } n \in \mathcal{N} \setminus \mathcal{N}^{\rm s}, \end{cases} \tag{4}$$

where β_n is the frequency bias factor of bus $n \in \mathcal{N}$. It depends on the frequency characteristics of the generator and the load connected to bus n [34]. In particular, the generator at bus n can be modeled by its speed-droop characteristic ϕ_n. The load at bus n can be modeled by its damping coefficient ψ_n. The frequency bias factor of bus n is $\beta_n = 1/\phi_n + \psi_n$.

b) ESS's Operation Model: The power demand of the ESS at bus $n \in \mathcal{N}^s$ in time slot $t \in \mathcal{T}$ has limits $p_n^{\rm s,\,min} < 0$ and $p_n^{\rm s,\,max} > 0$. We have

$$p_n^{\rm s,\,min} \le p_n^{\rm s}(t) \le p_n^{\rm s,\,max}. \tag{5}$$

Note that $p_n^{\rm s}(t) < 0$ (or > 0) indicates that the ESS is discharging (or charging). The change in the charging/discharging power of the ESS at bus $n \in \mathcal{N}^s$ is subject to the ramp up and down rating limits $\Delta p_n^{\rm s,\,min} < 0$ and $\Delta p_n^{\rm s,\,max} > 0$, respectively. For $t \in \mathcal{T} \setminus \{1\}$, we have

$$\Delta p_n^{\rm s,\,min} \le p_n^{\rm s}(t) - p_n^{\rm s}(t-1) \le \Delta p_n^{\rm s,\,max}. \tag{6}$$

Let $10\% \le SOC_n^{\rm init} \le 90\%$ and $E_n^{\rm s,\,max} \ge 0$ denote the initial state of charge (SOC) and the maximum capacity of the ESS at bus $n \in \mathcal{N}^{\rm s}$, respectively. Let $0 < e_n^{\rm s,\,c} \le 1$ and $0 < e_n^{\rm s,\,d} \le 1$ denote the energy transfer efficiency for charging and discharging the ESS at bus $n \in \mathcal{N}^{\rm s}$, respectively. We introduce slack variables $p_n^{\rm s,\,c}(t)$ and $p_n^{\rm s,\,d}(t)$ to indicate the charging and discharging power of the ESSs at bus $n \in \mathcal{N}^{\rm s}$ in time slot $t \in \mathcal{T}$, respectively, as given by

$$p_n^{\rm s}(t) = p_n^{\rm s,\,c}(t) - p_n^{\rm s,\,d}(t), \tag{7a}$$

$$0 \le p_n^{\rm s,\,c}(t) \le p_n^{\rm s,\,max}, \tag{7b}$$

$$0 \le p_n^{\rm s,\,d}(t) \le p_n^{\rm s,\,max}. \tag{7c}$$

Denote the SOC of the ESS at bus $n \in \mathcal{N}^{\rm s}$ in time slot $t \in \mathcal{T}$ by $SOC_n(t)$, the ESS's system dynamics can be updated by

$$SOC_n(t) = SOC_n(t-1) + \frac{1}{E_n^{\rm s,\,max}} \left(p_n^{\rm s,\,c}(t) e_n^{\rm s,\,c} - \frac{p_n^{\rm s,\,d}(t)}{e_n^{\rm s,\,d}} \right) \Delta t \times 100\%, \tag{8}$$

where $SOC_n(0) = SOC_n^{\rm init}$. The SOC level of the ESS at bus $n \in \mathcal{N}^{\rm s}$ in time slot $t \in \mathcal{T}$ is bounded by the lower and upper SOC limit, denoted by $SOC_n^{\rm min}$ and $SOC_n^{\rm max}$, respectively. We have

$$SOC_n^{\rm min} \le SOC_n(t) \le SOC_n^{\rm max}. \tag{9}$$

Constraints (5)−(9) guarantee that the ESSs operate within their physical range when providing frequency regulation.

B. Distribution Network Model

We consider the nonconvex AC power flow model and apply linear approximation to solve it in a timely fashion. Let $\boldsymbol{p}^{\rm inj}(t) = (p_n^{\rm inj}(t), n \in \mathcal{N})$ and $\boldsymbol{q}^{\rm inj}(t) = (q_n^{\rm inj}(t), n \in \mathcal{N})$ denote the vectors of injected active power $p_n^{\rm inj}(t)$ and reactive power $q_n^{\rm inj}(t)$ into bus $n \in \mathcal{N}$ in time slot $t \in \mathcal{T}$, respectively. Let $\boldsymbol{v}(t) = (|v_n(t)|, n \in \mathcal{N})$ and $\boldsymbol{\theta}(t) = (\theta_n(t), n \in \mathcal{N})$

This article has been accepted for publication in a future issue of this journal, but has not been fully edited. Content may change prior to final publication. Citation information: DOI 10.1109/TSG.2019.2920362, IEEE Transactions on Smart Grid

denote the vectors of voltage magnitude $|v_n(t)|$ and phase angle $\theta_n(t)$ of bus $n \in \mathcal{N}$ in time slot $t \in \mathcal{T}$, respectively. Let G_{nm} and B_{nm} denote the real and reactive parts of the entry (nm) in bus admittance matrix Y, respectively. Let b_{nn} and g_{nn} denote the shunt susceptance and conductance at bus n, respectively. The linearized AC power flow model in time slot t is given by [35]

$$\begin{bmatrix} \boldsymbol{p}^{\text{inj}}(t) \\ \boldsymbol{q}^{\text{inj}}(t) \end{bmatrix} = \begin{bmatrix} -\boldsymbol{B}' & \boldsymbol{G}' \\ -\boldsymbol{G} & -\boldsymbol{B} \end{bmatrix} \begin{bmatrix} \boldsymbol{\theta}(t) \\ \boldsymbol{v}(t) \end{bmatrix}, \tag{10}$$

where the nth diagonal element of matrices $\boldsymbol{B}$ and $\boldsymbol{B}'$ is B_{nn} and $B_{nn} - b_{nn}$, respectively. The non-diagonal entry (nm) of $\boldsymbol{B}$ and $\boldsymbol{B}'$ is B_{nm}. Similarly, the nth diagonal element of matrices $\boldsymbol{G}$ and $\boldsymbol{G}'$ is G_{nn} and $G_{nn} - g_{nn}$, respectively, and the non-diagonal entry (nm) of $\boldsymbol{G}$ and $\boldsymbol{G}'$ is G_{nm}.

In time slot t, the linearized active and reactive power flow through line $(n,m) \in \mathcal{L}$ with resistance R_{nm} and reactance X_{nm} can be obtained as [35]

$$p_{nm}(t) = \frac{R_{nm}\left(|v_n(t)| - |v_m(t)|\right) + X_{nm}(\theta_n(t) - \theta_m(t))}{R_{nm}^2 + X_{nm}^2}, \tag{11a}$$

$$q_{nm}(t) = \frac{X_{nm}\left(|v_n(t)| - |v_m(t)|\right) - R_{nm}(\theta_n(t) - \theta_m(t))}{R_{nm}^2 + X_{nm}^2}. \tag{11b}$$

The apparent power flow $s_{nm}(t) = \sqrt{p_{nm}^2(t) + q_{nm}^2(t)}$ is upper bounded by $s_{nm}^{\max}$. Its circular boundary can be linearized by a piecewise approximation using a regular polygon with central angle α. We have

$$p_{nm}(t)\cos(h\alpha) + q_{nm}(t)\sin(h\alpha) \le s_{nm}^{\max},\ (n,m) \in \mathcal{L}, \tag{12}$$

where $h = \{0, 1, \ldots, 2\pi/\alpha\}$. The voltage magnitude at bus n in time slot t is bounded by the limits $v_n^{\min}$ and $v_n^{\max}$. We have

$$v_n^{\min} \le |v_n(t)| \le v_n^{\max}, \quad n \in \mathcal{N}. \tag{13}$$

Constraints (10)–(13) determine the feasible power flow in time slot t and should be satisfied during frequency regulation.

III. Problem Formulation and Algorithm Design

In this section, we discuss how the system operator can regulate the frequency deviation at the transmission level by using the ESSs in the distribution network. On one hand, the system operator needs to restore the frequency when necessary, considering the uncertain frequency changes and the distribution network constraints. On the other hand, the ESSs seek to optimize their operation objective from frequency regulation, subject to their own operation constraints. The realized outcome of the system operator's frequency regulation decision depends on the ESSs' decision to participate in the regulation service. Therefore, we formulate a bi-level optimization problem with a chance constraint to account for uncertain frequency changes. Since the system operator may have limited knowledge about the ESSs' operation information (e.g., the ESS cost function), we propose a decentralized algorithm which allows the system operator to achieve consensus with the ESSs on frequency regulation decisions without knowing the ESSs' operation information. We prove that the optimal solution of the decentralized algorithm converges to the solution of the centralized optimization problem.

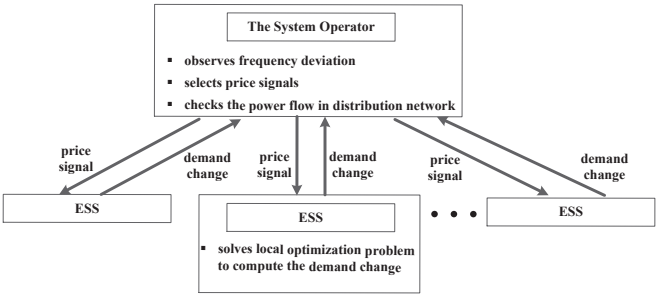

Fig. 1. The bi-level decision making and the information exchange between the system operator and the ESSs.

The bi-level decision making and the information exchange between the system operator and the ESSs are illustrated in Fig. 1. The system operator and the ESSs are the decision makers at the upper and lower level, respectively. At the upper level, the system operator observes the frequency deviation, selects the price signal and sends it to the ESSs, and then makes sure the distribution network constraints are satisfied when performing frequency regulation. At the lower level, each ESS makes a decision on its participation based on the price signal, and informs the system operator about its decision on the demand change for the regulation service. This enables the system operator at the upper level and the ESSs at the lower level to pursue their own objectives, while taking into account the operation constraints and aligning on the frequency regulation decisions.

A. ESS's Local Problem

At the beginning of every control time slot, each ESS can make a decision on whether to participate in the regulation service or not. A cost will incur for any ESSs that decide to participate, as they need to adjust their power demand to provide the regulation service. The cost can be compensated by the revenue that the ESSs receive from the system operator for providing frequency regulation. Given the assumption that ESSs are rational and self-interested, they aim to maximize the profit from participating in the regulation service.

The revenue of the ESSs is defined as the reward from the system operator for their participation in the regulation service. At the beginning of time slot $t \in \mathcal{T}$, the system operator issues a price signal $\varrho_n^{\text{s}}(t) \in \mathbb{R}$ to indicate whether it needs regulation down or up service from the ESS at bus $n \in \mathcal{N}^{\text{s}}$, depending on the current frequency deviation. If the system operator needs regulation down capacity from the ESS at bus $n \in \mathcal{N}^{\text{s}}$, it sends a positive price signal $\varrho_n^{\text{s}}(t) > 0$ to the ESS at bus n. If the ESS decides to participate, it will respond by either increasing its charging rate or decreasing its discharging rate to provide a power demand change $\Delta p_n^{\text{s}}(t) > 0$ for regulation down service. Similarly, if the system operator needs regulation up capacity from the ESS at bus $n \in \mathcal{N}^{\text{s}}$, it sends a negative price signal $\varrho_n^{\text{s}}(t) < 0$ to the ESS at bus n. If the ESS decides to participate, the ESS will respond by either decreasing its charging rate or increasing its discharging rate to provide a power demand change $\Delta p_n^{\text{s}}(t) < 0$ for regulation up service.

This article has been accepted for publication in a future issue of this journal, but has not been fully edited. Content may change prior to final publication. Citation information: DOI 10.1109/TSG.2019.2920362, IEEE Transactions on Smart Grid

The revenue of the ESS at bus n from providing frequency regulation in time slot t can be given as

$$f_n^{\text{s,rev}}\left(\Delta p_n^{\text{s}}(t)\right) = \varrho_n^{\text{s}}(t)\Delta p_n^{\text{s}}(t). \tag{14}$$

The cost of the ESSs consists of two components, i.e., the ESSs schedule change as well as the associated energy loss from changing their power demand to provide frequency regulation. To define the cost for the ESSs schedule change, we note that the ESSs expect to have diminishing returns by disrupting their own demand schedule to provide the regulation service. In other words, the marginal cost of the ESSs to provide frequency regulation will increase with their power demand change. For the ESS at bus $n \in \mathcal{N}^{\text{s}}$, we define its cost $C_n^{\text{dis}}(\Delta p_n^{\text{s}}(t))$ from schedule change for frequency regulation in time slot $t \in \mathcal{T}$ as follows

$$C_n^{\text{dis}}(\Delta p_n^{\text{s}}(t)) = a_n \|\Delta p_n^{\text{s}}(t)\|_2^2, \tag{15}$$

where $\|\cdot\|_2$ is the l_2-norm and a_n is a positive coefficient. Note that the coefficient a_n captures the different responses of the ESSs to the scheduled demand change for providing the regulation service. It represents the level of dissatisfaction of the ESS at bus n as a function of its power demand change. The quadratic cost function (15) is an empirical approximation of the ESS operation in practice, which is also commonly used in the literature for modelling load utility and user comfort levels [36]–[38]. It captures the disruption level of the ESS schedule at bus $n \in \mathcal{N}^{\text{s}}$. Note that if the ESS at bus $n \in \mathcal{N}^{\text{s}}$ follows the scheduled demand in time slot $t \in \mathcal{T}$, there is no cost incurred, i.e., $C_n(\Delta p_n^{\text{s}}(t)) = 0$ when $\Delta p_n^{\text{s}}(t) = 0$.

Remark 1: The cost function (15) is nonnegative, differentiable, and strictly convex in $\Delta p_n^{\text{s}}(t)$.

The energy loss of the ESSs from changing their power demand to provide frequency regulation is given by

$$C_n^{\text{loss}}(\Delta p_n^{\text{s}}(t)) = (1 - e_n^{\text{s,c}})p_n^{\text{s,c}}(t) + \left(\frac{1}{e_n^{\text{s,d}}} - 1\right) p_n^{\text{s,d}}(t) - \text{C}_n^{\text{sch}}. \tag{16}$$

Note that the first and second terms in the energy loss function (16) capture the energy loss from charging and discharging the ESS at bus $n \in \mathcal{N}^{\text{s}}$ in time slot $t \in \mathcal{T}$, respectively. The last term in the energy loss function (16) captures the energy loss from the scheduled power demand of the ESS at bus n in time slot $t \in \mathcal{T}$, such that we have $C_n^{\text{loss}}(\Delta p_n^{\text{s}}(t)) = 0$ if the ESS at bus $n \in \mathcal{N}^{\text{s}}$ follows the scheduled demand in time slot $t \in \mathcal{T}$. Therefore, the total cost of the ESS at bus $n \in \mathcal{N}^{\text{s}}$ in time slot $t \in \mathcal{T}$ for frequency regulation is given by

$$C_n(\Delta p_n^{\text{s}}(t)) = C_n^{\text{dis}}(\Delta p_n^{\text{s}}(t)) + C_n^{\text{loss}}(\Delta p_n^{\text{s}}(t)). \tag{17}$$

Each ESS aims to maximize its total profit from participating in the regulation service during the current time slot t and the upcoming time slots $\tau \in \mathcal{T}(t+1) = \{t+1, \ldots, T\}$. Let $\Delta \boldsymbol{p}_n^{\text{s}}(t) = (\Delta p_n^{\text{s}}(t), \ldots, \Delta p_n^{\text{s}}(T))$ denote the decision variable vector of the ESS at bus $n \in \mathcal{N}^{\text{s}}$ in time slot $t \in \mathcal{T}$, its objective function is given by

$$f_n^{\text{s,obj}}\left(\Delta \boldsymbol{p}_n^{\text{s}}(t)\right) = \sum_{\tau \in \mathcal{T}(t)} \left(f_n^{\text{s,rev}}\left(\Delta p_n^{\text{s}}(\tau)\right) - C_n(\Delta p_n^{\text{s}}(\tau))\right). \tag{18}$$

We denote the price information for the ESS at bus $n \in \mathcal{N}^{\text{s}}$ in current time slot $t \in \mathcal{T}$ and the upcoming time slots $\tau \in \mathcal{T}(t+1)$ by a price vector $\boldsymbol{\varrho}_n^{\text{s}}(t) = \left(\varrho_n^{\text{s}}(t), \ldots, \varrho_n^{\text{s}}(T)\right)$. If $\boldsymbol{\varrho}_n^{\text{s}}(t)$ is given by the system operator at time slot $t \in \mathcal{T}$, the ESS at bus $n \in \mathcal{N}^{\text{s}}$ can solve a local optimization problem to maximize its profit, while satisfying its operation constraints. Let $\mathcal{P}_n^{\text{s}}(t)$ denote the feasible space defined by constraints (5)−(9) for operating the ESS at bus $n \in \mathcal{N}^{\text{s}}$ in time slot $t \in \mathcal{T}$. The local problem for the ESS at bus n in time slot t can be formulated as

$$\underset{\Delta \boldsymbol{p}_n^{\text{s}}(t)}{\text{maximize}} \quad f_n^{\text{s,obj}}\left(\Delta \boldsymbol{p}_n^{\text{s}}(t)\right) \tag{19a}$$

$$\text{subject to} \quad p_n^{\text{s}}(\tau) \in \mathcal{P}_n^{\text{s}}(\tau), \quad \tau \in \mathcal{T}(t). \tag{19b}$$

Note that problem (19) is strongly convex in the decision variable vector $\Delta \boldsymbol{p}_n^{\text{s}}(t)$. The feasible space $\mathcal{P}_n^{\text{s}}(t)$ defined by constraints (5)−(9) is convex and compact. Thus, a unique solution exists for problem (19) given the price vector $\boldsymbol{\varrho}_n^{\text{s}}(t)$. We denote this unique solution by $\Delta \boldsymbol{p}_n^{\text{s}*}(t) = \mathcal{B}_n^{\text{s}}\left(\boldsymbol{\varrho}_n^{\text{s}}(t)\right)$, which captures the optimal response of the ESS at bus n in time slot t with respect to price vector $\boldsymbol{\varrho}_n^{\text{s}}(t)$.

We note that the ESS at bus $n \in \mathcal{N}^{\text{s}}$ is guaranteed to be either charging or discharging in time slot t to provide frequency regulation, as well as to satisfy the ramp up or down limits. At optimality, the cost function (16) guarantees that we must have either $\Delta p_n^{\text{s,c}}(\tau) = 0$ or $\Delta p_n^{\text{s,c}}(\tau) = 0, \tau \in \mathcal{T}(t)$. Otherwise, we can reduce $\Delta p_n^{\text{s,c}}(\tau)$ and $\Delta p_n^{\text{s,d}}(\tau), \tau \in \mathcal{T}(t)$ by the same amount $\delta_p(\tau), \tau \in \mathcal{T}(t)$ to preserve feasibility. However, the profit will increase by $\sum_{\tau \in \mathcal{T}(t)}(1 - e_n^{\text{s,c}})\delta_p(\tau) + \sum_{\tau \in \mathcal{T}(t)}(1/e_n^{\text{s,d}} - 1)\delta_p(\tau)$, which contradicts with the optimality condition. This indicates that the ESS at bus n can only be either charging or discharging in time slot t to provide frequency regulation. Further with constraints (6) and (7a), the ESS at bus n is also guaranteed to satisfy the ramp up or down limits when providing the regulation service.

B. System Operator's Centralized Problem

At the beginning of time slot $t \in \mathcal{T}$, the system operator observes the frequency deviation $\Delta\omega(t)$ at the transmission level and makes a decision for frequency regulation by using the ESSs in the distribution network. The system operator aims to regulate the frequency deviation in current time slot t. However, the regulated frequency $|\Delta\omega(t) + \Delta\omega^{\text{reg}}(t)|$ depends on the ESSs' participation to provide the system frequency change $\Delta\omega^{\text{reg}}(t)$, which is affected by the ESSs' profits from providing the regulation service. To align with the interests of the ESSs, the system operator needs to address the ESSs' profit along with its frequency regulation objective.

The system operator also needs to account for the future risk of the frequency deviation when making the decision in current time slot t, since the ESSs have limited energy storage. However, the system operator is uncertain about the frequency changes $\Delta\omega(\tau)$ in the upcoming time slots $\tau \in \mathcal{T}(t+1)$. To tackle the uncertainty in system frequency changes, the system operator can use a chance constraint to enforce a low probability of frequency deviation after performing frequency

This article has been accepted for publication in a future issue of this journal, but has not been fully edited. Content may change prior to final publication. Citation information: DOI 10.1109/TSG.2019.2920362, IEEE Transactions on Smart Grid

regulation using the ESSs. We have

$$\mathbb{P}\big(|\Delta\omega(\tau)+\Delta\omega^{\text{reg}}(\tau)|\le\epsilon,\ \tau\in\mathcal{T}(t+1)\big)\ge 1-\sigma, \quad (20)$$

where $\mathbb{P}(A)$ denotes the probability of event A, and $\sigma\in[0,1)$ is the maximum regulated frequency deviation probability the system operator can tolerate. In practice, the system operator can choose σ based on its tolerance for the regulated frequency deviation in the upcoming time slots, considering the ESSs or other available resources for frequency regulation.

Moreover, the system operator needs to ensure that the operation constraints imposed by the distribution network are satisfied when performing frequency regulation during current time slot t and the upcoming time slots $\tau\in\mathcal{T}(t+1)$. Let $\boldsymbol{\psi}(t)=\big(\Delta p_n^{\text{s}}(\tau),\, n\in\mathcal{N}^{\text{s}},\, \Delta\omega^{\text{reg}}(\tau),\, \boldsymbol{p}^{\text{inj}}(\tau),\, \boldsymbol{q}^{\text{inj}}(\tau),\, \boldsymbol{\theta}(\tau),\, \boldsymbol{v}(\tau),\, \tau\in\mathcal{T}(t)\big)$ denote the decision variable vector. The centralized optimization problem for the system operator in time slot $t\in\mathcal{T}$ can be formulated as

$$\underset{\substack{\boldsymbol{\psi}(t),\,\varrho_n^{\text{s}}(\tau),\\ n\in\mathcal{N}^{\text{s}},\,\tau\in\mathcal{T}(t)}}{\text{minimize}} \sum_{\tau\in\mathcal{T}(t)}\sum_{n\in\mathcal{N}^{\text{s}}} C_n(\Delta p_n^{\text{s}}(\tau))+\kappa|\Delta\omega(t)+\Delta\omega^{\text{reg}}(t)| \quad (21a)$$

$$\text{subject to}\quad |\Delta\omega(t)+\Delta\omega^{\text{reg}}(t)|\le\epsilon, \quad (21b)$$

$$\text{constraint (20)},$$

$$\Delta p_n^{\text{s}}(\tau)=\mathcal{B}_n^{\text{s}}\left(\varrho_n^{\text{s}}(\tau)\right), n\in\mathcal{N}^{\text{s}},\,\tau\in\mathcal{T}(t), \quad (21c)$$

$$\text{constraints (3), (4), and (10)}-\text{(13)}$$

$$\text{for time slots } \{t,\dots,T\}, \quad (21d)$$

where κ is a positive weight coefficient parameter. The objective function (21a) captures the ESSs' profit in the first term as well as the system operator's frequency regulation objective in the second term. Note that the first term in (21a) only includes the ESSs' cost function, as the reward received by the ESSs cancels out with the reward paid by the system operator. The weight coefficient κ allows the system operator to trade-off between the ESSs' profit and its frequency regulation objective. Constraint (21b) guarantees the regulated frequency deviation in the current time slot t is within the acceptable range required by the system operator. Constraints (20) and (21d) ensure the uncertainty in the system frequency changes and its impact on the system operation in the upcoming time slots $\tau\in\mathcal{T}(t+1)$ have been addressed by the system operator.

Problem (21) is a bi-level chance-constrained optimization problem, where the system operator and the ESSs are the decision maker at the upper and lower levels, respectively. The optimal strategy of each ESS is included in problem (21) through constraint (21c), i.e., the system operator takes into account the responses from the ESSs toward any given price vector $\boldsymbol{\varrho}_n^{\text{s}}(t)$ when making decisions. The system operator solves problem (21) and sends the optimal price vector $\boldsymbol{\varrho}_n^{\text{s}*}(t)$ to the ESS at bus $n\in\mathcal{N}^{\text{s}}$. Subsequently, the ESS at bus n responds with the power demand changes $\Delta\boldsymbol{p}_n^{\text{s}*}(t)$ from solving its local problem (19) based on the price vector from the system operator.

It is difficult for the system operator to solve problem (21), as the chance constraint (20) is nonconvex. The coupling constraint (21c) is also nonconvex, even though it is convex in variable $\Delta\boldsymbol{p}_n^{\text{s}*}(t)$ and $\boldsymbol{\varrho}_n^{\text{s}}(t)$ separately. Moreover, it may not be even practical for the system operator to solve problem (21), as the coupling constraint (21c) requires the ESSs to share all their operation information (e.g., ESSs' cost function) with the system operator for frequency regulation. However, some ESSs may choose to keep some information local for privacy concerns. In the following subsection, we tackle these challenges in solving problem (21). First, we address the nonconvex chance constraint (20) by using the scenario approximation technique. Then, we tackle the coupling constraint (21c) by designing appropriate price signals. Finally, we propose a decentralized algorithm such that the ESSs privacy preference can be accommodated, while the frequency regulation objective is also achieved.

C. Convex Relaxation and Algorithm Design

We first address the nonconvex chance constraint (20). Chance constraints can be handled by an approximation approach such as the Bernstein approximation [39]. However, this requires the probability distribution function of the frequency deviation, which may not be available. In this paper, we adopt the scenario approximation approach that does not require the explicit information about the frequency deviation distribution to tackle the chance constraint [40], [41]. In particular, we approximate the chance constraint by using a set $\mathcal{J}\triangleq\{1,\dots,J\}$ of J frequency samples $\Delta\boldsymbol{\omega}^j(t+1)=\big(\Delta\omega^j(t+1),\dots,\Delta\omega^j(T)\big)$ of the random variable $\Delta\boldsymbol{\omega}(t+1)=(\Delta\omega(t+1),\dots,\Delta\omega(T))$ in the upcoming time slots $\tau\in\mathcal{T}(t+1)=\{t+1,\dots,T\}$, as given by

$$\left|\Delta\omega^j(\tau)+\Delta\omega^{\text{reg}}(\tau)\right|\le\epsilon,\ \tau\in\mathcal{T}(t+1),\ j\in\mathcal{J}. \quad (22)$$

By replacing the chance constraint (20) with the convex approximation (22), the system operator solves the following optimization problem instead

$$\underset{\substack{\boldsymbol{\psi}(t),\,\varrho_n^{\text{s}}(\tau),\\ n\in\mathcal{N}^{\text{s}},\,\tau\in\mathcal{T}(t)}}{\text{minimize}} \sum_{\tau\in\mathcal{T}(t)}\sum_{n\in\mathcal{N}^{\text{s}}} C_n(\Delta p_n^{\text{s}}(\tau))+\kappa|\Delta\omega(t)+\Delta\omega^{\text{reg}}(t)| \quad (23)$$

$$\text{subject to}\quad \text{constraints (21b)}-\text{(21d) and (22)}.$$

Problem (23) approximates the chance constraint with a finite number of convex constraints by using randomization over J realizations of the uncertain vector $\Delta\boldsymbol{\omega}(t+1)$. Note that the solution to problem (23) should satisfy the chance constraint (20) with a high probability, i.e., the solution to problem (23) is a feasible solution to problem (21) with a high confidence level. Thus, we are interested in the number of scenarios that is considered to be large enough to approximate the chance constraint. Reference [40] gives a bound on the number of scenarios required for the approximation based on Chernoff's inequality. This bound is tight when $\sigma=1/2$, but may not work well for the extreme values of σ [42], such as the σ that we need for the chance constraint to be satisfied with high probability. By following the work in [42], we derive a better bound that is tight at the extreme value of σ.

Lemma 1: Let M denote the number of variables in the chance constraint. For any $\delta\in(0,1)$, the solution of problem (23) will

This article has been accepted for publication in a future issue of this journal, but has not been fully edited. Content may change prior to final publication. Citation information: DOI 10.1109/TSG.2019.2920362, IEEE Transactions on Smart Grid

satisfy the chance constraint (20) with a probability not less than $1-\delta$, by selecting the number of scenarios as

$$J^* = \left\lceil \frac{M-1}{z} \right\rceil, \tag{24}$$

where z is the solution of

$$\begin{aligned} &z\log z + (1-z)\log(1-z) \\ &= z\left(\log\sigma - \log(1-\sigma) - \frac{\ln\delta}{M-1}\right) + \log(1-\sigma). \end{aligned} \tag{25}$$

Note that the $\log$ function in the base 2, and $\ln$ is the natural log function. The proof can be found in Appendix A.

Remark 2: The proposed scenario approximation approach does not rely on any assumptions on the frequency sample process and the frequency sample space. It is easy to be implemented and integrated in standard operation practice, as the system frequency measurements are already collected in current practice to monitor the system operation.

Next, we address the coupling constraint (21c). We relax constraint (21c) with a convex constraint in the problem formulation. We prove the optimal solution of the relaxed problem is also the optimal solution of the original problem, i.e., the relaxation gap is zero.

Let $\Delta\mathcal{P}_n^{\rm s}(\tau), \tau \in \mathcal{T}(t)$ denote the feasible space defined by constraints (2) and (19b). By replacing constraint (21c) with the convex constraint $\Delta p_n^{\rm s}(\tau) \in \Delta\mathcal{P}_n^{\rm s}(\tau), \tau \in \mathcal{T}(t)$, we relax problem (23) to the following optimization problem

$$\underset{\boldsymbol{\psi}(t)}{\text{minimize}} \sum_{\tau\in\mathcal{T}(t)} \sum_{n\in\mathcal{N}^{\rm s}} C_n(\Delta p_n^{\rm s}(\tau)) + \kappa|\Delta\omega(t) + \Delta\omega^{\rm reg}(t)| \tag{26a}$$

$$\text{subject to} \quad \Delta p_n^{\rm s}(\tau) \in \Delta\mathcal{P}_n^{\rm s}(\tau),\ \tau\in\mathcal{T}(t),\ n\in\mathcal{N}^{\rm s}, \tag{26b}$$
$$\text{constraints (21b), (21d), and (22).}$$

Problem (26) is a single-level convex optimization problem and can be solved efficiently. Given the strict convexity of its objective function, there exists a unique optimal solution for the ESSs power demand change $\Delta\boldsymbol{p}_n^{\rm s*}(t),\ n\in\mathcal{N}^{\rm s}$ that the system operator needs to restore the system frequency.

Remark 3: The solution of problem (26) is also the optimal solution of problem (23), under an appropriate price signal. The details are discussed as follows.

Problem (26) obtains the optimal solution $\Delta\boldsymbol{p}_n^{\rm s*}(t)$ by relaxing the feasible space of problem (23) and not including the price vector as the decision variable. If the solution of problem (26) is also in the feasible space of problem (23), the system operator needs to determine an appropriate price signal for problem (23) to obtain the same optimal $\Delta\boldsymbol{p}_n^{\rm s*}(t)$. That is, the system operator needs to find the optimal price vector $\boldsymbol{\varrho}_n^{\rm s*}(t)$ such that the ESSs decide to provide $\Delta\boldsymbol{p}_n^{\rm s*}(t) = \mathcal{B}_n^{\rm s}\left(\boldsymbol{\varrho}_n^{\rm s*}(t)\right), n\in\mathcal{N}^{\rm s}$ from solving their local optimization problem. As discussed below, we can prove such $\boldsymbol{\varrho}_n^{\rm s*}(t)$ exists for problem (23), and hence, the relaxation gap between problems (26) and (23) is zero.

For the system operator to determine the price vector $\boldsymbol{\varrho}_n^{\rm s*}(t)$, we first transform problem (26) into an equivalent problem by introducing a nonnegative auxiliary variable $\gamma(t)$ for the term $|\Delta\omega(t)+\Delta\omega^{\rm reg}(t)|$, as given by

$$\underset{\boldsymbol{\psi}(t),\gamma(t)}{\text{minimize}} \quad \sum_{\tau\in\mathcal{T}(t)}\sum_{n\in\mathcal{N}^{\rm s}} C_n(\Delta p_n^{\rm s}(\tau)) + \kappa\gamma(t) \tag{27a}$$

$$\text{subject to} \quad -\gamma(t) \le \Delta\omega(t) + \Delta\omega^{\rm reg}(t) \le \gamma(t), \tag{27b}$$

$$-\epsilon \le \Delta\omega(t) + \Delta\omega^{\rm reg}(t) \le \epsilon, \tag{27c}$$

$$-\epsilon \le \Delta\omega^j(\tau) + \Delta\omega^{\rm reg}(\tau) \le \epsilon,$$
$$\tau\in\mathcal{T}(t+1),\ j\in\mathcal{J}, \tag{27d}$$
$$\text{constraints (21d) and (26b).}$$

We introduce dual variables $\overline{\eta}^{\gamma}(t)$ and $\underline{\eta}^{\gamma}(t)$ for constraint (27b), dual variables $\overline{\lambda}^{\omega}(t)$ and $\underline{\lambda}^{\omega}(t)$ for constraint (27c), and dual variables $\overline{\zeta}^{j}(\tau)$ and $\underline{\zeta}^{j}(\tau), \tau\in\mathcal{T}(t+1), j\in\mathcal{J}$ for constraint (27d). Let superscript $*$ denote the value of the associated dual variables at the optimal solution of problem (27). We have the following theorem.

Theorem 1: The system operator can set a price vector $\boldsymbol{\varrho}_n^{\rm s*}(t)$ such that the optimal solution of problem (27) is also the optimal solution of problem (23). In particular, the price vector is given by

$$\varrho_n^{\rm s*}(t) = \frac{\underline{\eta}^{\gamma*}(t) - \overline{\eta}^{\gamma*}(t) + \underline{\lambda}^{\omega*}(t) - \overline{\lambda}^{\omega*}(t)}{\beta_{\mathcal{N}}},\ n\in\mathcal{N}^{\rm s}, \tag{28}$$

$$\varrho_n^{\rm s*}(\tau) = \sum_{j\in\mathcal{J}} \frac{\underline{\zeta}^{j*}(\tau) - \overline{\zeta}^{j*}(\tau)}{\beta_{\mathcal{N}}},\ n\in\mathcal{N}^{\rm s},\ \tau\in\mathcal{T}(t+1), \tag{29}$$

where $\beta_{\mathcal{N}} = \sum_{n\in\mathcal{N}}\beta_n$, and the dual variables $\overline{\eta}^{\gamma*}(t)$ and $\underline{\eta}^{\gamma*}(t)$ must satisfy

$$\underline{\eta}^{\gamma*}(t) + \overline{\eta}^{\gamma*}(t) = \kappa, \text{ if } \Delta\omega(t) + \Delta\omega^{\rm reg*}(t) = 0, \tag{30a}$$

$$\underline{\eta}^{\gamma*}(t) = \kappa,\ \overline{\eta}^{\gamma*}(t) = 0, \text{ if } 0 < \Delta\omega(t) + \Delta\omega^{\rm reg*}(t) \le \epsilon, \tag{30b}$$

$$\underline{\eta}^{\gamma*}(t) = 0,\ \overline{\eta}^{\gamma*}(t) = \kappa, \text{ if } -\epsilon \le \Delta\omega(t) + \Delta\omega^{\rm reg*}(t) < 0. \tag{30c}$$

The proof can be found in Appendix B. Based on Theorem 1, the system operator can use a decentralized approach to solve the problem in a distributed and iterative fashion. The decentralized approach enables the system operator to achieve consensus with the ESSs on the frequency regulation decision, without any knowledge on the cost function and operation constraints of the ESSs. In this paper, we design a decentralized algorithm for the system operator based on the projected subgradient method, as given in Algorithm 1. In each control time slot t, Algorithm 1 is executed in an iterative fashion to determine the amount of change in the ESSs power demand to provide frequency regulation. Let $\boldsymbol{\phi}(t) = \Big(\overline{\lambda}^{\omega}(t), \underline{\lambda}^{\omega}(t), \overline{\lambda}^{j}(\tau),\ j\in\mathcal{J}, \tau\in\mathcal{T}(t+1), \underline{\lambda}^{j}(\tau),\ j\in\mathcal{J}, \tau\in\mathcal{T}(t+1)\Big)$ denote the dual variable vector. We define $\boldsymbol{\Lambda}(t) = \Bigg(\Big(\Delta\omega(t) - \frac{1}{\beta_{\mathcal{N}}}\sum_{n\in\mathcal{N}^{\rm s}}\Delta p_n^{\rm s}(t) - \epsilon\Big), \Big(-\Delta\omega(t) + \frac{1}{\beta_{\mathcal{N}}}\sum_{n\in\mathcal{N}^{\rm s}}\Delta p_n^{\rm s}(t) - \epsilon\Big), \Big(\Delta\omega^j(\tau) - \frac{1}{\beta_{\mathcal{N}}}\sum_{n\in\mathcal{N}^{\rm s}}\Delta p_n^{\rm s}(\tau) - \epsilon\Big), j\in\mathcal{J}, \tau\in\mathcal{T}(t+1), \Big(-\Delta\omega^j(\tau) + \frac{1}{\beta_{\mathcal{N}}}\sum_{n\in\mathcal{N}^{\rm s}}\Delta p_n^{\rm s}(\tau) - \epsilon\Big), j\in\mathcal{J}, \tau\in\mathcal{T}(t+1)\Bigg)$.

This article has been accepted for publication in a future issue of this journal, but has not been fully edited. Content may change prior to final publication. Citation information: DOI 10.1109/TSG.2019.2920362, IEEE Transactions on Smart Grid

Algorithm 1 Decentralized Algorithm of Using ESSs for Frequency Regulation Executed in Time Slot t

1: Set $k := 1$.
2: The system operator initializes the power flow $\boldsymbol{p}_k^{\text{inj}}(t), \boldsymbol{q}_k^{\text{inj}}(t)$, $\boldsymbol{\theta}_k(t), \boldsymbol{v}_k(t)$ in the distribution network. Each ESS initializes its power demand $\boldsymbol{p}_{n,k}^{\text{s}}(t), n \in \mathcal{N}^{\text{s}}$, sets its upper and lower SOC limit, and calculates its energy loss from the scheduled demand.
3: The system operator observes the current frequency deviation $\Delta\omega(t)$, determines the number of samples needed based on (24) and (25), and generates the set $\mathcal{J}$ of J samples $\Delta\boldsymbol{\omega}^j(t+1), \forall j \in \mathcal{J}$ from the historical records. The system operator initializes the dual variables $\underline{\eta}_k^{\gamma}(t)$, $\overline{\eta}_k^{\gamma}(t)$, $\boldsymbol{\phi}_k(t)$.
4: **Repeat**
5: Each ESS $n \in \mathcal{N}^{\text{s}}$ sends the amount of change in its energy demand $\Delta\boldsymbol{p}_{n,k}^{\text{s}}(t)$ to the system operator.
6: The system operator updates the dual variables using (30) and (31), and sends the price vector $\boldsymbol{\varrho}_{n,k}^{\text{s}}(t)$ to the corresponding ESS at bus $n \in \mathcal{N}^{\text{s}}$.
7: The ESS at bus $n \in \mathcal{N}^{\text{s}}$ updates its energy demand change $\Delta\boldsymbol{p}_{n,k+1}^{\text{s}}(t)$ by solving problem (19).
8: The system operator checks the feasibility of the power flow in the distribution network based on (10)−(13).
9: $k := k + 1$.
10: **Until the algorithm converges**

Let k denote the iteration index. Let $\boldsymbol{\phi}_k(t)$ denote the dual variable vector at the kth iteration. The update can be obtained by

$$\boldsymbol{\phi}_{k+1}(t) = [\boldsymbol{\phi}_k(t) + \xi_k \boldsymbol{\Lambda}(t)]_{\wp}, \tag{31}$$

where ξ_k is the step size, and $[\cdot]_{\wp}$ is the projection onto the feasible space defined by $\overline{\lambda}^{\omega}(t) \geq 0, \underline{\lambda}^{\omega}(t) \geq 0, \overline{\lambda}^{j}(\tau) \geq 0$, $j \in \mathcal{J}$, $\tau \in \mathcal{T}(t+1)$, and $\underline{\lambda}^{j}(\tau) \geq 0, j \in \mathcal{J}, \tau \in \mathcal{T}(t+1)$.

In Algorithm 1, the initialization phase is in Lines 1 and 2. In each time slot t, the scheduled power demand and distribution network power flow are used by the ESSs and system operator to initialize their decision variables, respectively. Each ESS also sets its upper and lower SOC limits, and calculates the energy loss from their scheduled power demand. The selection of the realized frequency samples from the historical record is in Line 3. Lines 4 to 10 describe the frequency regulation process, during which the system operator and ESSs update their decisions in an iterative fashion. The information change between the ESSs and system operator is in Line 5. Each ESS decides the amount of demand change that it can provide for frequency regulation and sends it to the system operator. The dual variables and the price vector are updated in Line 6. The system operator uses the ESSs' demand change to update the price vectors and then sends the new price signal to the ESSs. The update of the corresponding power demand change in the ESSs is in Line 7. Based on the new price signal, each ESS updates its decision of the demand change for regulation service. The distribution network constraints are checked in Line 8. Given the updated ESSs demand change, the system operator computes the power flow changes in the distribution network and ensures that the constraints are satisfied. Finally, the iteration index is updated in Line 9.

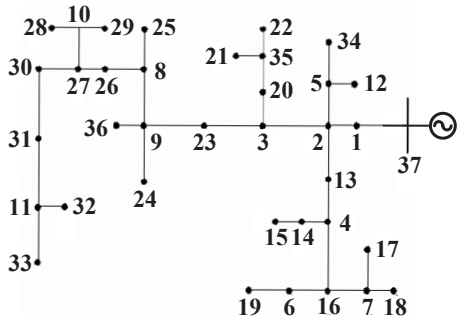

Fig. 2. The IEEE 37-bus distribution test feeder.

IV. Performance Evaluation

We evaluate the performance of the proposed frequency regulation approach on IEEE 37-bus and 123-bus distribution test feeders [43]. For demonstration, we present the settings of the IEEE 37-bus test feeder, as shown in Fig. 2. The voltage magnitudes are in per-unit (pu) with a 4.8 kV base. The base power of the system is 100 kVA. The slack bus is the substation bus 37, i.e., its voltage magnitude is 1 pu and its phase angle is zero. The substation bus is connected to an equivalent virtual generator to model the transmission network. We assume that there is no generator or frequency sensitive load within the 37-bus distribution network. We set the frequency bias factor of the substation bus to be an equivalent frequency bias factor for the distribution network, i.e., $\beta_n = 0$, $n = 1, \ldots, 36$, and $\beta_{37} = 3.483$ [34, p. 24]. The equivalent frequency bias factor at the substation bus represents the frequency response characteristic of the 37-bus test feeder in responses to the frequency regulation for the system operator at the transmission level. It captures the capability of the ESSs within the distribution network to provide or absorb energy when a disturbance happens and frequency deviates. Similarly, the settings of IEEE 123-bus test feeder can be determined by following the specifications in [43]. The energy transfer efficiency for charging and discharging the ESSs is set to be 0.95 [44]. The lower and upper SOC limits of the ESSs are set to be 10% and 90%, respectively. We consider a six-hour operation period, and divide it into 24 frequency control time slots with equal length of 15 minutes. We obtain the load profile from [45], and scale the load demand to make the average demand at each bus over the operation cycle equal to its corresponding spot load specified in [43]. We set the confidence level δ to be 0.1, and calculate the number of required frequency realizations $J = 70$. We obtain the samples of frequency deviation from [46]. The maximum acceptable steady-state frequency deviation ϵ is set to 0.05 for the current time slot, and 0.1 for the upcoming time slots. Unless stated otherwise, the weight coefficient a_n, $n \in \mathcal{N}^{\text{s}}$ for the ESSs' cost function and κ for the frequency regulation objective is set to be 3 and 1, respectively.

We first present the performance of our proposed decentralized algorithm for frequency regulation using three ESSs located at buses 13, 23, and 31, as shown in Fig. 3. We consider the case when the system operator has complete knowledge about the ESSs' operation information and the system frequency changes as the benchmark solution. As illustrated, the system

This article has been accepted for publication in a future issue of this journal, but has not been fully edited. Content may change prior to final publication. Citation information: DOI 10.1109/TSG.2019.2920362, IEEE Transactions on Smart Grid

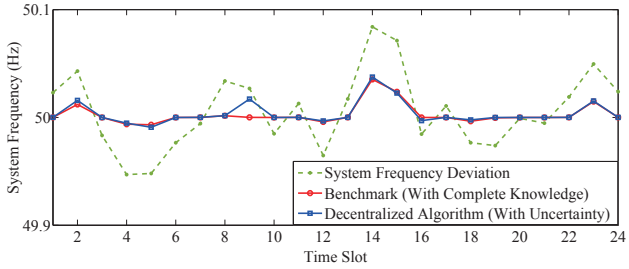

Fig. 3. Frequency regulation using three ESSs located at buses 13, 23, and 31, with sizes $E_{13}^{\max} = 200$ kWh, $E_{23}^{\max} = 150$ kWh, and $E_{31}^{\max} = 100$ kWh, respectively.

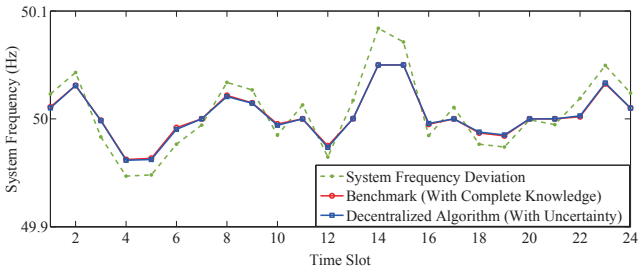

Fig. 4. Frequency regulation using an equivalent ESS located at bus 13 with $E_{13}^{\max} = 450$ kWh.

operator can achieve similar frequency regulation outcome without knowledge about the ESSs' operation information and about the frequency changes, except in a few time slots such as 2 and 9, when the system encounters some severe frequency changes and the ESSs may need to reverse their charging or discharging process to provide the regulation services. We then replace these three ESSs with a single ESS of equivalent total storage size located at bus 13 to provide frequency regulation. The frequency regulation outcome is illustrated in Fig. 4. It can be observed that the frequency regulation performance deteriorates in most of the time slots during the operation cycle, e.g. during time slots 4 to 15 and 22 to 23, with respect to the scenario of using three ESSs for frequency regulation. The limiting factor in this case arises from the power flow constraints in the distribution network, which limits the ESSs' participation in the regulation service. Note that we observe similar frequency regulation outcomes of our algorithm compared to the benchmark solution in this case.

To further study how the distribution network constraints affect the flexibility of using ESSs to achieve frequency regulation, we consider the same set of ESSs located at bus 13, 23, and 31, but with different sizes. We compare the total regulated frequency deviation after performing frequency regulation, as illustrated in Fig. 5. On the 37-bus test feeder, the regulated frequency deviation decreases by 23% when doubling the size of the ESSs. When tripling the size of the ESSs, the regulated frequency deviation decreases by 25%. The outcome of further reducing the regulated frequency deviation on 37-bus test feeder from increasing the ESSs storage are limited, due to the power flow limits of the distribution lines. For comparison, we also evaluate the frequency regulation performance when the same set of ESSs with different sizes are located at a larger test feeder, i.e., at bus 57, 83, and 149 on the 123-bus test feeder system. As illustrated in Fig. 5, we observe similar outcomes with respect to the 37-bus test feeder case. Therefore, we

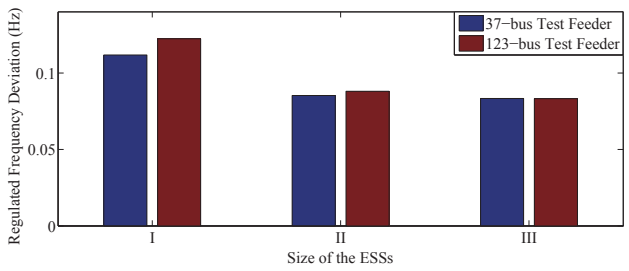

Fig. 5. Frequency regulation with three ESSs of different sizes on 37-bus and 123-bus test feeders: I) $E_{13}^{\max} = 200$ kWh, $E_{23}^{\max} = 150$ kWh, and $E_{31}^{\max} = 100$ kWh, II) $E_{13}^{\max} = 400$ kWh, $E_{23}^{\max} = 300$ kWh, and $E_{31}^{\max} = 200$ kWh, and III) $E_{13}^{\max} = 600$ kWh, $E_{23}^{\max} = 450$ kWh, and $E_{31}^{\max} = 300$ kWh, respectively.

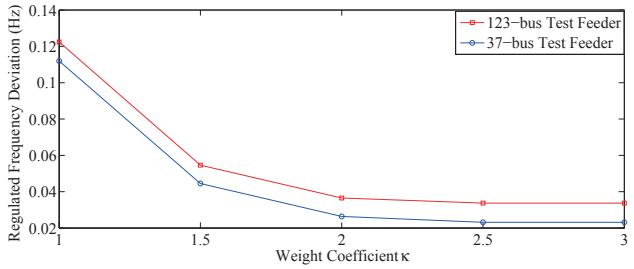

(a)

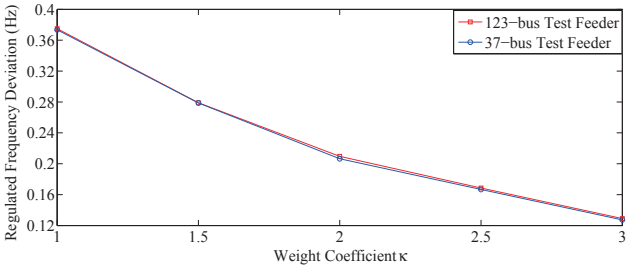

(b)

Fig. 6. Frequency regulation on 37-bus test feeder and 123-bus test feeder with different weight coefficients κ (a) using three ESSs, and (b) using a single ESS.

conclude that the distribution network constraints will affect the performance when using the ESSs to provide frequency regulation. It is more effective for the system operator to make use of smaller ESSs that are scattered in the distribution network to regulate the frequency deviation than relying on a single larger ESS.

As shown in Fig. 6, we also study the impact of the weight coefficient κ on the frequency regulation performance on both 37-bus and 123-bus test feeders. The results are obtained using the same set of ESSs in Fig. 3 and an equivalent ESS in Fig. 4, respectively. In both cases, it can be observed that the regulated system frequency deviation decreases as the weight coefficient κ increases, as the system operator increases the weight on its frequency regulation objective and tries to exploit the ESSs storage to a full extent to regulate the frequency deviation. We note that using three smaller size ESSs for frequency regulation always outperforms using one large equivalent ESS, as observed earlier in Figs. 3 and 4. This observation holds for both 37-bus and 123-bus test feeder cases. Moreover, it can be observed that using three ESSs on the 37-bus test feeder for frequency regulation constantly outperforms the same set of ESSs on the 123-bus test feeder. However, when

This article has been accepted for publication in a future issue of this journal, but has not been fully edited. Content may change prior to final publication. Citation information: DOI 10.1109/TSG.2019.2920362, IEEE Transactions on Smart Grid

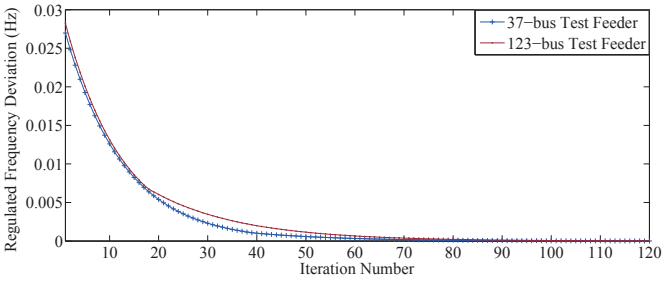

Fig. 7. The convergence of regulated system frequency deviation in control time slot $t = 1$ on 37-bus and 123-bus test feeders

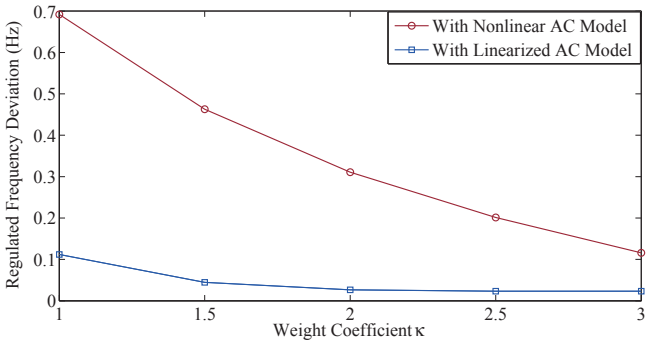

Fig. 8. Frequency regulation by using 3 ESSs on 37-bus test feeder with different weight coefficients κ based on linearized and nonlinear AC models.

a single equivalent ESS is used for frequency regulation, the performance on the 37-bus and 123-bus test feeders is similar. We reiterate that the distribution network constraints affect the ESSs' participation in frequency regulation. It is of practical value for the system operator to address the power flow constraints when performing frequency regulation.

Moreover, we note that our proposed decentralized algorithm can successfully converge to the centralized optimization problem of the system operator. We demonstrate the convergence of the regulated system frequency by illustrating the iterative process, when the same set of ESSs in Fig. 3 participate in the regulation service and make the decision in time slot $t = 1$. As shown in Fig. 7, the regulated system frequency converges after 90 iterations by using Algorithm 1 for both 37-bus and 123-bus test feeders. We thus note that our proposed decentralized algorithm can scale well from a smaller 37-bus test feeder to a larger 123-bus test feeder.

Finally, we compare the performance using the same set of ESSs in Fig. 3 for frequency regulation with the nonlinear AC power flow model when different weight coefficients κ are selected, as illustrated in Fig. 8. The nonlinear AC power flow model for the 37-bus test feeder is set up by using the MatPower toolbox [47], [48]. It can be observed that the performance deteriorates due to the power losses with the nonlinear AC model. With κ increases, the gap between the regulation performances with linearized and nonlinear power flow model shrinks. This indicates that the frequency regulation performance of our proposed method based on the linearized AC power flow model will be affected by the power loss in the actual distribution network. We note that the system operator can partially offset the power loss impact when implementing our proposed method in practical settings by increasing the weight on frequency regulation objective.

V. Conclusion

In this paper, we examined how the ESSs in the distribution network can participate in and contribute to the frequency regulation for the system operator at the transmission level. We addressed the operation objective of the ESSs when optimizing the frequency regulation decision for the system operator. We considered the uncertainty in the frequency changes, the availability of the ESSs, as well as the operation constraints imposed by the distribution network for frequency regulation service. In particular, we formulated a bi-level chance-constrained program for the system operator to align with the ESSs on frequency regulation decisions, using a chance constraint to account for the uncertain frequency changes. We proposed a decentralized algorithm such that the ESSs and system operator can pursue their own objectives, while ensuring frequency deviation is regulated and the distribution network constraints are satisfied. Simulation results validated our approach and demonstrated its effectiveness in assisting the system operator to achieve frequency regulation without knowledge about the ESSs' operation information, considering the uncertain frequency changes as well as the distribution network constraints. However, we note that the selected frequency bias factor may not be the actual representation of distribution network. The performance of our method will be affected by the power loss in the actual distribution networks.

There can be several directions for future work. First, it is worth further investigating how to measure the frequency bias factor and how to offset the power losses of the actual distribution network. Second, it is an interesting extension to understand how the system operator can interact with multiple distribution networks with different frequency response strategies. Third, another direction is to consider the bidding strategy of the self-interested ESSs to participate in electricity market, where the system operator takes into account the distribution network constraints for frequency regulation.

Appendix

A. Deriving the Bound on the Sample Generation

Problem (23) can be considered as a finite instance of the original problem (21), which approximates the nonconvex chance constraint with a set of J convex constraints. Let $\Delta\boldsymbol{\omega}_J^{\text{reg}}(t+1) = \left(\Delta\omega_J^{\text{reg}}(t+1), \ldots, \Delta\omega_J^{\text{reg}}(T)\right)$ denote an optimal solution to problem (23). By definition, if $\mathbb{P}\left(\left|\Delta\boldsymbol{\omega}(t+1) + \Delta\boldsymbol{\omega}_J^{\text{reg}}(t+1)\right| \le \epsilon\right) \ge 1-\sigma$, $\Delta\boldsymbol{\omega}_J^{\text{reg}}(t+1)$ satisfies the chance constraint (20) and is a solution of the original problem (21). For notation simplicity, we define

$$\Theta\left(\Delta\boldsymbol{\omega}_J^{\text{reg}}(t+1)\right) = \mathbb{P}\left(\left|\Delta\boldsymbol{\omega}(t+1) + \Delta\boldsymbol{\omega}_J^{\text{reg}}(t+1)\right| \le \epsilon\right), t \in \mathcal{T}. \quad (32)$$

Note that $\Theta\left(\Delta\boldsymbol{\omega}_J^{\text{reg}}(t+1)\right)$ is a random variable, as $\Delta\boldsymbol{\omega}_J^{\text{reg}}(t+1)$ depends on the number of J samples randomly chosen from the realizations of the random variable $\Delta\boldsymbol{\omega}(t+1) = \left(\Delta\omega(t+1), \ldots, \Delta\omega(T)\right)$. The larger J is, the higher the probability that $\Delta\boldsymbol{\omega}_J^{\text{reg}}(t+1)$ will satisfy the chance constraint (20) and the likelihood of $\Theta\left(\Delta\boldsymbol{\omega}_J^{\text{reg}}(t+1)\right) \ge 1-\sigma$ is higher. We thus aim to find the lower bound of the frequency sample number

This article has been accepted for publication in a future issue of this journal, but has not been fully edited. Content may change prior to final publication. Citation information: DOI 10.1109/TSG.2019.2920362, IEEE Transactions on Smart Grid

J that is considered large enough as a significant measure of the random variable $\Delta\boldsymbol{\omega}(t+1)$, such that a given observation of $\Delta\boldsymbol{\omega}(t+1)$ is also in the set of the J selected samples most of the times. In this case, if $\Delta\boldsymbol{\omega}_J^{\text{reg}}(t+1)$ satisfies constraint (22), it should satisfy the chance constraint (20) with high probability.

By using the results in [40], we can quantify the likelihood of $\Theta\big(\Delta\boldsymbol{\omega}_J^{\text{reg}}(t+1)\big) \geq 1-\sigma$, given the number of J frequency samples used to solve problem (23). We have

$$\mathbb{P}\left(\Theta\big(\Delta\boldsymbol{\omega}_J^{\text{reg}}(t+1)\big) \geq 1-\sigma\right) \geq 1-\sum_{i=0}^{M-1}\binom{J}{i}\sigma^i(1-\sigma)^{J-i}, \tag{33}$$

where $\binom{J}{i} = \dfrac{J!}{i!(J-i)!}$. Equation (33) can be interpreted that the solution of problem (23) is also feasible for the original problem (21), i.e., satisfies the chance constraint (20) with a probability not less than $1-\sum_{i=0}^{M-1}\binom{J}{i}\sigma^i(1-\sigma)^{J-i}$. Thus, given a confidence parameter $\delta \in (0,1)$, we can compute the minimum number J^* of the frequency realizations to be sampled such that $\mathbb{P}\left(\Theta\big(\Delta\boldsymbol{\omega}_J^{\text{reg}}(t+1)\big) \geq 1-\sigma\right) \geq 1-\delta$ if $J \geq J^*$, by using equation (33). The lower bound on the number of samples J can be derived as follows:

Lemma 1 For any $\sigma \in (0,1)$ and $d \leq \sigma J$, we have [41]

$$\sum_{i=0}^{M-1}\binom{J}{i}\sigma^i(1-\sigma)^{J-i} \leq \exp\left(-JD\left(\frac{d}{J} \parallel \sigma\right)\right), \tag{34}$$

where $D\left(A \parallel B\right)$ denote the relative entropy between two Bernoulli distributions A and B. It is given by

$$D\left(\frac{d}{J} \parallel \sigma\right) = \frac{d}{J}\log\left(\frac{d}{\sigma J}\right) + \left(1-\frac{d}{J}\right)\log\left(\frac{1-\frac{d}{J}}{1-\sigma}\right). \tag{35}$$

Note that (34) gives a better bound at the extreme value σ that we need to consider for the chance constraint to be satisfied with high probability. According to (33), we have that if

$$\exp\left(-JD\left(\frac{M-1}{J} \parallel \sigma\right)\right) \leq \delta, \tag{36}$$

$\mathbb{P}\left(\Theta\big(\Delta\boldsymbol{\omega}_J^{\text{reg}}(t+1)\big) \geq 1-\sigma\right) \geq 1-\delta$ holds. Note that we cannot directly solve (36) to obtain J^*. We thus further simplify (36) to express the relationship between the samples J^* needed and the confidence level $1-\delta$. By taking natural logarithm on both sides and considering the case when equality is achieved, we have

$$-JD\left(\frac{M-1}{J} \parallel \sigma\right) = \ln\delta. \tag{37}$$

By defining $z = \dfrac{M-1}{J}$, we can rewrite (37) as

$$-\frac{M-1}{z}\left(z\log\left(\frac{z}{\sigma}\right) + (1-z)\log\left(\frac{1-z}{1-\sigma}\right)\right) = \ln\delta. \tag{38}$$

By rearranging (38), we have

$$z\log z + (1-z)\log(1-z) = z\left(\log\sigma - \log(1-\sigma) - \frac{\ln\delta}{M-1}\right) + \log(1-\sigma). \tag{39}$$

After selecting σ and δ, we can solve (39) to obtain z and J^* can given as

$$J^* = \left\lceil \frac{M-1}{z} \right\rceil. \tag{40}$$

B. Lagrangian Relaxation and Optimality Condition

We first tackle the coupling between variables $\Delta\omega^{\text{reg}}(t)$ and $\Delta p_n^{\text{s}}(t)$ in problem (27) by summing equation (4), where we leverage the relationship between them in each time slot $t \in \mathcal{T}$. Consider a lossless system, i.e., $\sum_{n\in\mathcal{N}}\Delta p_n^{\text{inj}}(t) = 0$, we have

$$\Delta\omega^{\text{reg}}(t) = -\frac{\sum_{n\in\mathcal{N}^{\text{s}}}\Delta p_n^{\text{s}}(t)}{\beta_{\mathcal{N}}}, \tag{41}$$

where $\beta_{\mathcal{N}} = \sum_{n\in\mathcal{N}}\beta_n$. Substituting $\Delta\omega^{\text{reg}}(t)$ by equation (41) and denoting the decision variables vector by $\boldsymbol{\psi}_{\text{LD}}(t) = \big(\Delta p_n^{\text{s}}(\tau),\, n\in\mathcal{N}^{\text{s}},\, \boldsymbol{p}^{\text{inj}}(\tau), \boldsymbol{q}^{\text{inj}}(\tau),\, \boldsymbol{\theta}(\tau),\, \boldsymbol{v}(\tau),\, \tau\in\mathcal{T}(t)\big)$, we can rewrite problem (27) as

$$\underset{\boldsymbol{\psi}_{\text{LD}}(t),\gamma(t)}{\text{minimize}} \quad \sum_{\tau\in\mathcal{T}(t)}\sum_{n\in\mathcal{N}^{\text{s}}} C_n(\Delta p_n^{\text{s}}(\tau)) + \kappa\gamma(t) \tag{42a}$$

$$\text{subject to} \quad -\gamma(t) \leq \Delta\omega(t) - \frac{\sum_{n\in\mathcal{N}^{\text{s}}}\Delta p_n^{\text{s}}(t)}{\beta_{\mathcal{N}}} \leq \gamma(t), \tag{42b}$$

$$-\epsilon \leq \Delta\omega(t) - \frac{\sum_{n\in\mathcal{N}^{\text{s}}}\Delta p_n^{\text{s}}(t)}{\beta_{\mathcal{N}}} \leq \epsilon, \tag{42c}$$

$$-\epsilon \leq \Delta\omega^j(\tau) - \frac{\sum_{n\in\mathcal{N}^{\text{s}}}\Delta p_n^{\text{s}}(\tau)}{\beta_{\mathcal{N}}} \leq \epsilon,$$
$$\tau\in\mathcal{T}(t+1),\, j\in\mathcal{J}, \tag{42d}$$

constraints (21d) and (26b).

Next we derive the partial Lagrangian function by using the defined dual variables, as given by

$$\begin{aligned}
&L(\gamma(t), \Delta\boldsymbol{p}_n^{\text{s}}(t)) \qquad (43)\\
&= \sum_{\tau\in\mathcal{T}(t)}\sum_{n\in\mathcal{N}^{\text{s}}} C_n\big(\Delta p_n^{\text{s}}(\tau)\big) + \kappa\gamma(t)\\
&\quad + \underline{\eta}^{\gamma}(t)\left(\Delta\omega(t) - \frac{\sum_{n\in\mathcal{N}^{\text{s}}}\Delta p_n^{\text{s}}(t)}{\beta_{\mathcal{N}}} - \gamma(t)\right)\\
&\quad + \overline{\eta}^{\gamma}(t)\left(-\Delta\omega(t) + \frac{\sum_{n\in\mathcal{N}^{\text{s}}}\Delta p_n^{\text{s}}(t)}{\beta_{\mathcal{N}}} - \gamma(t)\right)\\
&\quad + \underline{\lambda}^{\omega}(t)\left(\Delta\omega(t) - \frac{\sum_{n\in\mathcal{N}^{\text{s}}}\Delta p_n^{\text{s}}(t)}{\beta_{\mathcal{N}}} - \epsilon\right)\\
&\quad + \overline{\lambda}^{\omega}(t)\left(-\Delta\omega(t) + \frac{\sum_{n\in\mathcal{N}^{\text{s}}}\Delta p_n^{\text{s}}(t)}{\beta_{\mathcal{N}}} - \epsilon\right)\\
&\quad + \sum_{\tau\in\mathcal{T}(t+1)}\sum_{j\in\mathcal{J}}\underline{\zeta}^{j}(\tau)\left(\Delta\omega^j(\tau) - \frac{\sum_{n\in\mathcal{N}^{\text{s}}}\Delta p_n^{\text{s}}(\tau)}{\beta_{\mathcal{N}}} - \epsilon\right)\\
&\quad + \sum_{\tau\in\mathcal{T}(t+1)}\sum_{j\in\mathcal{J}}\overline{\zeta}^{j}(\tau)\left(-\Delta\omega^j(\tau) + \frac{\sum_{n\in\mathcal{N}^{\text{s}}}\Delta p_n^{\text{s}}(\tau)}{\beta_{\mathcal{N}}} - \epsilon\right).
\end{aligned}$$

The dual function, denoted by $f^{\text{dual}}(\gamma(t), \Delta\boldsymbol{p}_n^{\text{s}}(t))$, is

$f^{\text{dual}}(\gamma(t), \Delta\boldsymbol{p}_n^{\text{s}}(t))$

This article has been accepted for publication in a future issue of this journal, but has not been fully edited. Content may change prior to final publication. Citation information: DOI 10.1109/TSG.2019.2920362, IEEE Transactions on Smart Grid

$$= \inf_{\gamma(t),\Delta \boldsymbol{p}_n^{\mathrm{s}}(t)} \{L(\gamma(t), \Delta \boldsymbol{p}_n^{\mathrm{s}}(t)) \mid \text{constraints (21d) and (26b)}\}. \tag{44}$$

The dual problem is given by

$$\underset{\substack{\underline{\eta}^{\gamma}(t), \overline{\eta}^{\gamma}(t), \underline{\lambda}^{\omega}(t), \overline{\lambda}^{\omega}(t), \\ \underline{\zeta}^{j}(\tau), \overline{\zeta}^{j}(\tau), j\in\mathcal{J}, \tau\in\mathcal{T}(t+1)}}{\text{maximize}} \quad f^{\text{dual}}(\gamma(t), \Delta \boldsymbol{p}_n^{\mathrm{s}}(t)) \tag{45a}$$

$$\text{subject to} \quad \underline{\eta}^{\gamma}(t),\, \overline{\eta}^{\gamma}(t),\, \underline{\lambda}^{\omega}(t),\, \overline{\lambda}^{\omega}(t) \geq 0, \tag{45b}$$

$$\underline{\zeta}^{j}(\tau),\, \overline{\zeta}^{j}(\tau) \geq 0,\, j \in \mathcal{J},\, \tau \in \mathcal{T}(t+1). \tag{45c}$$

Given the strict convexity and Slater's condition holds, the optimal solution of the Lagrange dual problem is equal to the primal problem. Note that in the primal problem, the decision variable $\gamma(t)$ is the ancillary variable for the term $|\Delta\omega(t) + \Delta\omega^{\text{reg}}(t)| = \left|\Delta\omega(t) - \frac{\sum_{n\in\mathcal{N}^s} \Delta p_n^{\mathrm{s}}(t)}{\beta_{\mathcal{N}}}\right|$. The constraints (21d) and (26b) are only imposed on variable $\Delta p_n^{\mathrm{s}}(t)$, $n \in \mathcal{N}^s$. We first evaluate the optimality conditions of the variable $\gamma(t)$. At optimality, we can have either $\gamma^*(t) = 0$ or $\gamma^*(t) \neq 0$. When $\gamma^*(t)$ is equal to zero, we have

$$\begin{aligned} &\underline{\eta}^{\gamma *}(t) + \overline{\eta}^{\gamma *}(t) = \kappa, \\ &\text{if } \ \Delta\omega(t) + \Delta\omega^{\text{reg}*}(t) = 0. \end{aligned} \tag{46}$$

When $\gamma^*(t)$ is not equal to zero at optimality, we must have either $\gamma^*(t) = \Delta\omega(t) + \Delta\omega^{\text{reg}*}(t)$ or $\gamma^*(t) = -(\Delta\omega(t) + \Delta\omega^{\text{reg}*}(t))$. Otherwise, we can reduce $\gamma^*(t)$ by an amount $\Delta\gamma > 0$ but still preserve feasibility. The value of the objective function will be reduced by $\kappa\Delta\gamma$, which contradicts the optimality condition. Therefore, we have either

$$\begin{aligned} &\underline{\eta}^{\gamma *}(t) = \kappa, \overline{\eta}^{\gamma *}(t) = 0, \\ &\text{if } \ 0 < \Delta\omega(t) + \Delta\omega^{\text{reg}*}(t) \leq \epsilon, \end{aligned} \tag{47}$$

or

$$\begin{aligned} &\underline{\eta}^{\gamma *}(t) = 0, \overline{\eta}^{\gamma *}(t) = \kappa, \\ &\text{if } \ -\epsilon \leq \Delta\omega(t) + \Delta\omega^{\text{reg}*}(t) < 0. \end{aligned} \tag{48}$$

Next, we discuss the optimality condition of $\Delta \boldsymbol{p}_n^{\mathrm{s}}(t), n \in \mathcal{N}^{\mathrm{s}}$. Note that $\gamma^*(t) = \left|\Delta\omega^*(t) - \frac{\sum_{n\in\mathcal{N}^s} \Delta p_n^{\mathrm{s}}(t)}{\beta_{\mathcal{N}}}\right|$ always holds at optimality. By leveraging the aforementioned relationship, we can rewrite the partial Lagrangian function only with respect to the variable $\Delta \boldsymbol{p}_n^{\mathrm{s}}(t), n \in \mathcal{N}^{\mathrm{s}}$. We have

$$\begin{aligned} &L(\Delta \boldsymbol{p}_n^{\mathrm{s}}(t)) \\ &= \sum_{\tau\in\mathcal{T}(t)} \sum_{n\in\mathcal{N}^{\mathrm{s}}} C_n\big(\Delta p_n^{\mathrm{s}}(\tau)\big) \\ &\quad + \underline{\eta}^{\gamma}(t)\left(\Delta\omega(t) - \frac{\sum_{n\in\mathcal{N}^{\mathrm{s}}} \Delta p_n^{\mathrm{s}}(t)}{\beta_{\mathcal{N}}}\right) \\ &\quad + \overline{\eta}^{\gamma}(t)\left(-\Delta\omega(t) + \frac{\sum_{n\in\mathcal{N}^{\mathrm{s}}} \Delta p_n^{\mathrm{s}}(t)}{\beta_{\mathcal{N}}}\right) \\ &\quad + \underline{\lambda}^{\omega}(t)\left(\Delta\omega(t) - \frac{\sum_{n\in\mathcal{N}^{\mathrm{s}}} \Delta p_n^{\mathrm{s}}(t)}{\beta_{\mathcal{N}}} - \epsilon\right) \\ &\quad + \overline{\lambda}^{\omega}(t)\left(-\Delta\omega(t) + \frac{\sum_{n\in\mathcal{N}^{\mathrm{s}}} \Delta p_n^{\mathrm{s}}(t)}{\beta_{\mathcal{N}}} - \epsilon\right) \end{aligned} \tag{49}$$

$$\begin{aligned} &+ \sum_{\tau\in\mathcal{T}(t+1)} \sum_{j\in\mathcal{J}} \underline{\zeta}^{j}(\tau)\left(\Delta\omega^{j}(\tau) - \frac{\sum_{n\in\mathcal{N}^{\mathrm{s}}} \Delta p_n^{\mathrm{s}}(\tau)}{\beta_{\mathcal{N}}} - \epsilon\right) \\ &+ \sum_{\tau\in\mathcal{T}(t+1)} \sum_{j\in\mathcal{J}} \overline{\zeta}^{j}(\tau)\left(-\Delta\omega^{j}(\tau) + \frac{\sum_{n\in\mathcal{N}^{\mathrm{s}}} \Delta p_n^{\mathrm{s}}(\tau)}{\beta_{\mathcal{N}}} - \epsilon\right). \end{aligned}$$

Similarly, we rewrite the dual function

$$\begin{aligned} &f^{\text{dual}}(\Delta \boldsymbol{p}_n^{\mathrm{s}}(t)) \\ &= \inf_{\Delta \boldsymbol{p}_n^{\mathrm{s}}(t)} \{L(\Delta \boldsymbol{p}_n^{\mathrm{s}}(t)) \mid \text{constraints (21d) and (26b)}\}, \end{aligned} \tag{50}$$

and the dual problem is given by

$$\begin{aligned} &\underset{\substack{\underline{\eta}^{\gamma}(t), \overline{\eta}^{\gamma}(t), \underline{\lambda}^{\omega}(t), \overline{\lambda}^{\omega}(t), \\ \underline{\zeta}^{j}(\tau), \overline{\zeta}^{j}(\tau), j\in\mathcal{J}, \tau\in\mathcal{T}(t+1)}}{\text{maximize}} \quad f^{\text{dual}}(\Delta \boldsymbol{p}_n^{\mathrm{s}}(t)) \\ &\text{subject to} \quad \text{constraints (45b), (45c),} \\ &\qquad\qquad \text{and (46)}-\text{(48).} \end{aligned} \tag{51}$$

Note that the system operator needs to achieve consensus on the amount of demand change $\Delta \boldsymbol{p}_n^{\mathrm{s}}(t)$ with the ESS at bus $n \in \mathcal{N}^{\mathrm{s}}$. This can be accomplished if and only if the optimality condition for the ESS local problem is the same as the optimality condition for the Lagrange dual problem. Thus,

$$\frac{\partial L\left(\Delta \boldsymbol{p}_n^{\mathrm{s}}(t)\right)}{\partial p_n^{\mathrm{s}}(t)} = -\frac{\partial f_n^{\mathrm{s,obj}}(\Delta \boldsymbol{p}_n^{\mathrm{s}}(t))}{\partial p_n^{\mathrm{s}}(t)}, \tag{52}$$

$$\frac{\partial L\left(\Delta \boldsymbol{p}_n^{\mathrm{s}}(t)\right)}{\partial p_n^{\mathrm{s}}(\tau)} = -\frac{\partial f_n^{\mathrm{s,obj}}(\Delta \boldsymbol{p}_n^{\mathrm{s}}(t))}{\partial p_n^{\mathrm{s}}(\tau)}, \tau \in \mathcal{T}(t+1). \tag{53}$$

That is,

$$\frac{-\underline{\eta}^{\gamma *}(t) + \overline{\eta}^{\gamma *}(t) - \underline{\lambda}^{\omega *}(t) + \overline{\lambda}^{\omega *}(t)}{\beta_{\mathcal{N}}} = -\varrho_n^{\mathrm{s}*}(t), \tag{54}$$

$$-\sum_{j\in\mathcal{J}} \frac{\underline{\zeta}^{j*}(\tau) - \overline{\zeta}^{j*}(\tau)}{\beta_{\mathcal{N}}} = -\varrho_n^{\mathrm{s}*}(\tau),\, \tau \in \mathcal{T}(t+1). \tag{55}$$

By rearranging the above equations, we obtain the price signal

$$\varrho_n^{\mathrm{s}*}(t) = \frac{\underline{\eta}^{\gamma *}(t) - \overline{\eta}^{\gamma *}(t) + \underline{\lambda}^{\omega *}(t) - \overline{\lambda}^{\omega *}(t)}{\beta_{\mathcal{N}}}, \tag{56}$$

$$\varrho_n^{\mathrm{s}*}(\tau) = \sum_{j\in\mathcal{J}} \frac{\underline{\zeta}^{j*}(\tau) - \overline{\zeta}^{j*}(\tau)}{\beta_{\mathcal{N}}},\, \tau \in \mathcal{T}(t+1), \tag{57}$$

along with the conditions obtained earlier for the dual variables $\underline{\eta}^*(t)$ and $\overline{\eta}^*(t)$

$$\underline{\eta}^{\gamma *}(t) + \overline{\eta}^{\gamma *}(t) = \kappa, \text{ if } \Delta\omega(t) + \Delta\omega^{\text{reg}*}(t) = 0, \tag{58}$$

$$\underline{\eta}^{\gamma *}(t) = \kappa, \overline{\eta}^{\gamma *}(t) = 0, \text{ if } 0 < \Delta\omega(t) + \Delta\omega^{\text{reg}*}(t) \leq \epsilon, \tag{59}$$

$$\underline{\eta}^{\gamma *}(t) = 0, \overline{\eta}^{\gamma *}(t) = \kappa, \text{ if } -\epsilon \leq \Delta\omega(t) + \Delta\omega^{\text{reg}*}(t) < 0. \tag{60}$$

This completes the proof.

REFERENCES

[1] U.S. Department of Energy, "Maintaining reliability in the modern power system," Tech. Rep., Dec. 2016. [Online]. Available: https://energy.gov/sites/prod/files/2017/01/f34/MaintainingReliabilityintheModernPowerSystem.pdf

[2] D. Hedberg, M. Emnett, G. Sodeberg, N. McIntire, R. Gramlich, and R. Kondziolka, "FERC order 890: What does it mean for the west?" National Association of Regulatory Utility Commissioners (NARUC), National Wind Coordinating Collaborative (NWCC), and the Western Governors Association, Tech. Rep., Feb. 2007.

[3] U.S. Federal Energy Regulatory Commission (FERC), "Frequency regulation compensation in organized wholesale power markets," *Washington, DC, FERC 755, Dockets RM11-7-000 AD10-11-000*, Oct. 2011.

[4] M. Kintner-Meyer, "Regulatory policy and markets for energy storage in North America," in *Proc. of the IEEE*, vol. 102, no. 7, pp. 1065–1072, Jul. 2014.

[5] U.S. Federal Energy Regulatory Commission (FERC), "Electric storage participation in markets organized by regional transmission organizations and independent system operators," *Washington, DC, FERC 841, Dockets RM16-23-000 AD16-20-000*, Feb. 2018.

[6] M. C. Kintner-Meyer, P. J. Balducci, C. Jin, T. B. Nguyen, M. A. Elizondo, V. V. Viswanathan, X. Guo, and F. K. Tuffner, "Energy storage for power systems applications: A regional assessment for the northwest power pool (NWPP)," Apr. 2010. [Online]. Available: https://www.osti.gov/biblio/991590

[7] California ISO, "Advancing and maximizing the value of energy storage technology - A California roadmap," Dec. 2014. [Online]. Available: http://www.caiso.com/Documents/Advancing-MaximizingValueofEnergyStorageTechnology_CaliforniaRoadmap.pdf

[8] B. Xu, Y. Dvorkin, D. S. Kirschen, C. A. Silva-Monroy, and J. P. Watson, "A comparison of policies on the participation of storage in U.S. frequency regulation markets," in *Proc. of IEEE Power and Energy Society General Meeting*, Boston, MA, Jul. 2016.

[9] Y. Zhang, V. Gevorgian, C. Wang, X. Lei, E. Chou, R. Yang, Q. Li, and L. Jiang, "Grid-level application of electrical energy storage: Example use cases in the United States and China," *IEEE Power and Energy Mag.*, vol. 15, no. 5, pp. 51–58, Sept. 2017.

[10] C. Jin, N. Lu, S. Lu, Y. V. Makarov, and R. A. Dougal, "A coordinating algorithm for dispatching regulation services between slow and fast power regulating resources," *IEEE Trans. on Smart Grid*, vol. 5, no. 2, pp. 1043–1050, Mar. 2014.

[11] Y. Cheng, M. Tabrizi, M. Sahni, A. Povedano, and D. Nichols, "Dynamic available AGC based approach for enhancing utility scale energy storage performance," *IEEE Trans. on Smart Grid*, vol. 5, no. 2, pp. 1070–1078, Mar. 2014.

[12] S. Lee, J. Kim, C. Kim, S. Kim, E. Kim, D. Kim, K. K. Mehmood, and S. U. Khan, "Coordinated control algorithm for distributed battery energy storage systems for mitigating voltage and frequency deviations," *IEEE Trans. on Smart Grid*, vol. 7, no. 3, pp. 1713–1722, May 2016.

[13] F. Zhang, Z. Hu, X. Xie, J. Zhang, and Y. Song, "Assessment of the effectiveness of energy storage resources in the frequency regulation of a single-area power system," *IEEE Trans. on Power System*, vol. 32, no. 5, pp. 3373–3380, Sept. 2017.

[14] G. He, Q. Chen, C. Kang, Q. Xia, and K. Poolla, "Cooperation of wind power and battery storage to provide frequency regulation in power markets," *IEEE Trans. on Power Systems*, vol. 32, no. 5, pp. 3559–3568, Sept. 2017.

[15] J. Tan and Y. Zhang, "Coordinated control strategy of a battery energy storage system to support a wind power plant providing multi-timescale frequency ancillary services," *IEEE Trans. on Sustainable Energy*, vol. 8, no. 3, pp. 1140–1153, Jul. 2017.

[16] H. Mohsenian-Rad, "Optimal bidding, scheduling, and deployment of battery systems in California day-ahead energy market," *IEEE Trans. on Power Systems*, vol. 31, no. 1, pp. 442–453, Jan. 2016.

[17] S. Chen, T. Zhang, H. B. Gooi, R. D. Masiello, and W. Katzenstein, "Penetration rate and effectiveness studies of aggregated BESS for frequency regulation," *IEEE Trans. on Smart Grid*, vol. 7, no. 1, pp. 167–177, Jan. 2016.

[18] D. Fooladivanda, C. Rosenberg, and S. Garg, "Energy storage and regulation: An analysis," *IEEE Trans. on Smart Grid*, vol. 7, no. 4, pp. 1813–1823, Jul. 2016.

[19] T. A. Nguyen, R. H. Byrne, R. J. Concepcion, and I. Gyuk, "Maximizing revenue from electrical energy storage in MISO energy & frequency regulation markets," in *Proc. of IEEE Power Energy Society General Meeting*, Chicago, IL, Jul. 2017.

[20] Y. J. Zhang, C. Zhao, W. Tang, and S. H. Low, "Profit maximizing planning and control of battery energy storage systems for primary frequency control," *IEEE Trans. on Smart Grid*, vol. 9, no. 2, pp. 712–723, Mar. 2018.

[21] E. Nasrolahpour, S. J. Kazempour, H. Zareipour, and W. D. Rosehart, "Strategic sizing of energy storage facilities in electricity markets," *IEEE Trans. on Sustainable Energy*, vol. 7, no. 4, pp. 1462–1472, Oct. 2016.

[22] M. González Vayá and G. Andersson, "Optimal bidding strategy of a plug-in electric vehicle aggregator in day-ahead electricity markets under uncertainty," *IEEE Trans. on Power Systems*, vol. 30, no. 5, pp. 2375–2385, Sept. 2015.

[23] M. Yazdani-Damavandi, N. Neyestani, M. Shafie-khah, J. Contreras, and J. P. S. Catalão, "Strategic behavior of multi-energy players in electricity markets as aggregators of demand side resources using a bi-level approach," *IEEE Trans. on Power Systems*, vol. 33, no. 1, pp. 397–411, Jan. 2018.

[24] R. Mohammadi, H. R. Mashhadi, and M. Shahidehpour, "Market-based customer reliability provision in distribution systems based on game theory: A bi-level optimization approach," accepted for publication in *IEEE Trans. on Smart Grid*, 2018.

[25] M. Vrakopoulou, B. Li, and J. L. Mathieu, "Chance constrained reserve scheduling using uncertain controllable loads part I: Formulation and scenario-based analysis," *IEEE Trans. on Smart Grid*, vol. 10, no. 2, pp. 1608–1617, Mar. 2019.

[26] H. Zhang, Z. Hu, E. Munsing, S. J. Moura, and Y. Song, "Data-driven chance-constrained regulation capacity offering for distributed energy resources," accepted for publication in *IEEE Trans. on Smart Grid*, 2018.

[27] E. Yao, V. W. S. Wong, and R. Schober, "Optimization of aggregate capacity of PEVs for frequency regulation service in day-ahead market," *IEEE Trans. on Smart Grid*, vol. 9, no. 4, pp. 3519–3529, Jul. 2018.

[28] A. Ravichandran, S. Sirouspour, P. Malysz, and A. Emadi, "A chance-constraints-based control strategy for microgrids with energy storage and integrated electric vehicles," *IEEE Trans. on Smart Grid*, vol. 9, no. 1, pp. 346–359, Jan. 2018.

[29] J. Engels, B. Claessens, and G. Deconinck, "Combined stochastic optimization of frequency control and self-consumption with a battery," *IEEE Trans. on Smart Grid*, vol. 10, no. 2, pp. 1971–1981, Mar. 2019.

[30] H. Gerard, E. I. R. Puente, and D. Six, "Coordination between transmission and distribution system operators in the electricity sector: A conceptual framework," *Utilities Policy*, vol. 50, pp. 40–48, Feb. 2018.

[31] Y. Sun, S. Bahrami, V.W.S Wong, and L. Lampe, "Application of energy storage systems for frequency regulation service," in *Proc. of IEEE SmartGridComm*, Dresden, Germany, Oct. 2017.

[32] B. J. Kirby, "Frequency regulation basics and trends," U.S. Department of Energy, Dec. 2005.

[33] NERC, "Balancing and frequency control: A technical document prepared by the NERC resources subcommittee," Jan. 2011.

[34] H. Bevrani, *Robust Power System Frequency Control*. Springer, 2009.

[35] N. Cai, "Linearized and distributed methods for power flow analysis and control in smart grids and microgrids," Ph.D. dissertation, Dept. Electrical Eng., Michigan State University, 2014.

[36] C. Zhao, U. Topcu, N. Li, and S. Low, "Design and stability of load-side primary frequency control in power systems," *IEEE Trans. on Automatic Control*, vol. 59, no. 5, pp. 1177–1189, May 2014.

[37] P. Samadi, S. Bahrami, V. W. S. Wong, and R. Schober, "Power dispatch and load control with generation uncertainty," in *Proc. of IEEE Global Conference on Signal and Information Processing (GlobalSIP)*, Orlando, FL, Dec. 2015.

[38] P. Samadi, V. W. S. Wong, and R. Schober, "Load scheduling and power trading in systems with high penetration of renewable energy resources," *IEEE Trans. on Smart Grid*, vol. 7, no. 4, pp. 1802–1812, Jul. 2016.

[39] A. Nemirovski and A. Shapiro, "Convex approximations of chance constrained programs," *SIAM Journal on Optimization*, vol. 17, no. 4, pp. 969–996, Nov. 2006.

[40] A. M. C. So and Y. J. A. Zhang, "Distributionally robust slow adaptive OFDMA with soft QoS via linear programming," *IEEE J. on Selected Areas in Commun.*, vol. 31, no. 5, pp. 947–958, May 2013.

[41] A. Nemirovski and A. Shapiro, "Scenario approximations of chance constraints," in *Probabilistic and Randomized Methods for Design under Uncertainty*, G. Calafiore and F. Dabbene, Eds. Springer London, 2006, pp. 3–47.

[42] R. Arratia and L. Gordon, "Tutorial on large deviations for the binomial distribution," *Bulletin of Mathematical Biology*, vol. 51, no. 1, pp. 125–131, Jan. 1989.

[43] "IEEE Power and Energy Society distribution test feeders," 2016. [Online]. Available: http://ewh.ieee.org/soc/pes/dsacom/testfeeders/index.html

[44] Center for sustainable systems, University of Michigan, "U.S. grid energy storage," 2018. [Online]. Available: http://css.umich.edu/sites/default/files/U.S._Grid_Energy_Storage_Factsheet_CSS15-17_e2018.pdf

[45] IESO, "Hourly Ontario and market demands, year to date." [Online]. Available: www.ieso/power-data/data-directory

[46] FINGRID, "Frequency measurement data." [Online]. Available: http://www.fingrid.fi/en/powersystem/Powersystemmanagement/MaintainineofbalancebetweenelectricityconsumptionandproductionFrequencymeasurementsdata/Pages/default.aspx

[47] R. D. Zimmerman, C. E. Murillo-Sanchez, and R. J. Thomas, "MATPOWER: Steady-State operations, planning, and analysis tools for power systems research and education," *IEEE Trans. on Power Systems*, vol. 26, no. 1, pp. 12–19, Feb. 2011.

[48] C. E. Murillo-Snchez, R. D. Zimmerman, C. L. Anderson, and R. J. Thomas, "Secure planning and operations of systems with stochastic sources, energy storage, and active demand," *IEEE Trans. on Smart Grid*, vol. 4, no. 4, pp. 2220–2229, Dec. 2013.

Yanan Sun (S'14) received the B.S. degree in Information Engineering and M.S. degree in Systems Engineering from Xi'an Jiaotong University, Xi'an, China, in 2011 and 2014, respectively. She is currently a Ph.D. candidate in the Department of Electrical and Computer Engineering, The University of British Columbia (UBC), Vancouver, BC, Canada. Her research interests lie in the broad area of cyber-physical system. Her current work focuses on smart meter privacy and energy storage applications in smart grid.

Shahab Bahrami (S'12, M'17) received the B.Sc. and M.A.Sc. degrees both in Electrical Engineering from Sharif University of Technology, Tehran, Iran, in 2010 and 2012, respectively. He received the Ph.D. degree in Electrical & Computer Engineering from the University of British Columbia (UBC), Vancouver, BC, Canada in 2017. Dr. Bahrami continued to work as a post-doctoral research fellow at UBC until Jan. 2018. He also worked as a post-doctoral research fellow at the University of Tehran, Iran from May 2018 to Apr. 2019. Currently, he works as a post-doctoral research fellow at UBC. Dr. Bahrami has received various prestigious scholarships at UBC, including the distinguished and highly competitive UBCs Four Year Fellowship (2013 - 2017), and the Graduate Support Initiative Award from the Faculty of Applied Science at UBC (2014 - 2017). His research interests include power flow analysis, demand response, optimization, and algorithm design with applications to smart grid.

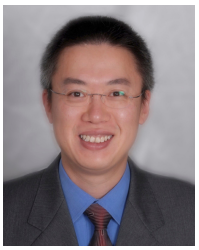

Vincent W.S. Wong (S'94, M'00, SM'07, F'16) received the B.Sc. degree from the University of Manitoba, Winnipeg, MB, Canada, in 1994, the M.A.Sc. degree from the University of Waterloo, Waterloo, ON, Canada, in 1996, and the Ph.D. degree from the University of British Columbia (UBC), Vancouver, BC, Canada, in 2000. From 2000 to 2001, he worked as a systems engineer at PMC-Sierra Inc. (now Microchip Technology Inc.). He joined the Department of Electrical and Computer Engineering at UBC in 2002 and is currently a Professor. His research areas include protocol design, optimization, and resource management of communication networks, with applications to wireless networks, smart grid, mobile edge computing, and Internet of Things. Currently, Dr. Wong is an Executive Editorial Committee Member of *IEEE Transactions on Wireless Communications*, an Area Editor of *IEEE Transactions on Communications*, and an Associate Editor of *IEEE Transactions on Mobile Computing*. He has served as a Guest Editor of *IEEE Journal on Selected Areas in Communications* and *IEEE Wireless Communications*. He has also served on the editorial boards of *IEEE Transactions on Vehicular Technology* and *Journal of Communications and Networks*. He was a Tutorial Co-Chair of *IEEE Globecom*18, a Technical Program Co-chair of *IEEE SmartGridComm*'14, as well as a Symposium Co-chair of *IEEE ICC*'18, *IEEE SmartGridComm* ('13, '17) and *IEEE Globecom*'13. He is the Chair of the IEEE Vancouver Joint Communications Chapter and has served as the Chair of the IEEE Communications Society Emerging Technical Sub-Committee on Smart Grid Communications. He received the 2014 UBC Killam Faculty Research Fellowship. He is an IEEE Communications Society Distinguished Lecturer (2019 - 2020).

Lutz Lampe (M02-SM08) received the Dipl.-Ing. and Dr.-Ing. degrees in electrical engineering from the University of Erlangen, Germany, in 1998 and 2002, respectively. Since 2003, he has been with the Department of Electrical and Computer Engineering, The University of British Columbia, Vancouver, BC, Canada, where he is a Full Professor. His research interests are broadly in theory and application of wireless, power line, optical wireless and optical fibre communications. Dr. Lampe is currently an Associate Editor for the IEEE TRANSACTIONS ON COMMUNICATIONS, the IEEE COMMUNICATIONS LETTERS, and the IEEE COMMUNICATIONS SURVEYS AND TUTORIALS. He was a (co-)recipient of a number of best paper awards, including awards at the 2006 IEEE International Conference on Ultra-Wideband (ICUWB), the 2010 IEEE International Communications Conference (ICC), and the 2011, 2017 and 2018 IEEE International Conference on Power Line Communications and Its Applications (ISPLC). In 2009, he received the Friedrich Wilhelm Bessel Award by the Alexander von Humboldt Foundation. He was the General (Co-)Chair for the 2005 IEEE ISPLC, the 2009 IEEE ICUWB and the 2013 IEEE International Conference on Smart Grid Communications (SmartGridComm). He has been a Distinguished Lecturer of the IEEE Communications Society in 2012-2013. He is a co-editor of the book Power Line Communications: Principles, Standards and Applications from Multimedia to Smart Grid, published by John Wiley & Sons in its 2nd edition in 2016.